

The Higgs Boson Sector of the Next-to-MSSM with CP Violation

Kingman Cheung^{a,b,c}, Tie-Jiun Hou^{a,b}, Jae Sik Lee^b, and Eibun Senaha^b

^a *Department of Physics, National Tsing Hua University, Hsinchu, Taiwan 300*

^b *Physics Division, National Center for Theoretical Sciences, Hsinchu, Taiwan 300*

^c *Division of Quantum Phases & Devices, Konkuk University, Seoul 143-701, Korea*

Abstract

We perform a comprehensive study of the Higgs sector in the framework of the next-to-minimal supersymmetric standard model with CP-violating parameters in the superpotential and in the soft-supersymmetry-breaking sector. Since the CP is no longer a good symmetry, the two CP-odd and the three CP-even Higgs bosons of the next-to-minimal supersymmetric standard model in the CP-conserving limit will mix. We show explicitly how the mass spectrum and couplings to gauge bosons of the various Higgs bosons change when the CP-violating phases take on nonzero values. We include full one-loop and the logarithmically enhanced two-loop effects employing the renormalization-group (RG) improved approach. In addition, the LEP limits, the global minimum condition, and the positivity of the square of the Higgs-boson mass have been imposed. We demonstrate the effects on the Higgs-mass spectrum and the couplings to gauge bosons with and without the RG-improved corrections. Substantial modifications to the allowed parameter space happen because of the changes to the Higgs-boson spectrum and their couplings with the RG-improved corrections. Finally, we calculate the mass spectrum and couplings of the few selected scenarios and compare to the previous results in literature where possible; in particular, we illustrate a scenario motivated by electroweak baryogenesis.

1 Introduction

Supersymmetry (SUSY) is the leading candidate for the physics beyond the standard model (SM). It not only solves the gauge hierarchy problem, but also provides a dynamical mechanism for electroweak symmetry breaking and a natural candidate for the dark matter. The minimal supersymmetric extension of the SM (MSSM) has attracted much phenomenological and theoretical interest but it suffers from the so-called little hierarchy problem and the μ problem.

An extension with an extra singlet superfield, known as the next-to-minimal supersymmetric standard model (NMSSM) [1–5] was motivated to provide a natural solution to the μ problem. The μ parameter in the term $\mu H_u H_d$ of the superpotential of the MSSM naturally has its value at either M_{Planck} or zero (due to a symmetry). However, the radiative electroweak symmetry breaking conditions require the μ parameter to be of the same order as the Z -boson mass for fine-tuning reasons. Such a conflict was coined as the μ problem [6]. In the NMSSM, the μ term is generated dynamically through the vacuum-expectation value (VEV), v_S , of the scalar component of the additional Higgs field S , which is naturally of the order of the SUSY-breaking scale. Thus, an effective μ parameter of the order of the electroweak scale is generated. The NMSSM was recently revived because it was shown that it can effectively relieve the little hierarchy problem [7]. Because of the additional Higgs singlet field and an approximate Peccei-Quinn (PQ) symmetry, the NMSSM naturally has a light pseudoscalar Higgs boson a_1 . It has been shown [7] that, in most parameter space that is natural, the SM-like Higgs boson can decay into a pair of light pseudoscalar bosons with a branching ratio larger than 0.7. Thus, the branching ratio of the SM-like Higgs boson into $b\bar{b}$ would be less than 0.3 and so the LEP II bound is effectively reduced to around 100 GeV [8]. Since the major decay modes of the Higgs boson are no longer $b\bar{b}$, unusual search modes have been investigated [9].

In SUSY models, CP-violating phases naturally appear in the μ term of the superpotential and in the soft-SUSY breaking terms. The nonobservation of electric dipole moments (EDMs) for thallium [10], neutron [11], and mercury [12,13] is known to constrain CP-violating phases very tightly. Nevertheless, cancellations among various contributions may occur among several contributions to the three measured EDMs, thus still allowing sizable CP phases [14,15]. In the MSSM, the nonvanishing CP phases could radiatively induce significant mixing between the CP-even and CP-odd states [16–19], giving rise to a number of interesting CP-violating phenomena and substantial modifications to Higgs-boson phenomenology [20,21]. In particular, the lightest Higgs boson can be as light as a few GeV with almost vanishing couplings to the weak gauge bosons when the CP-violating phases are maximal. The decay patterns of the heavier Higgs bosons become much more complicated compared to the CP-conserving case because of the loss of its CP parities [22,23]. These combined features make the Higgs boson-searches at LEP difficult; consequently, the

Higgs boson lighter than ~ 50 GeV can survive the LEP limit [24].

In this work, we study the NMSSM Higgs sector with CP violation. In the CP-conserving limit, the neutral Higgs sector in the NMSSM includes two CP-odd and three CP-even states. With CP violation the 5 neutral Higgs bosons lose their CP parities and all mix together. We anticipate a whole new set of phenomena associated with the singlet extension of the MSSM in the presence of nontrivial CP-violating phases in the VEVs, and the μ and soft SUSY-breaking parameters. As the first step toward this new extension, we calculate the whole mass spectrum of the Higgs sector as well as the couplings to the vector gauge bosons, which will dictate the production and decay patterns of the Higgs bosons. Phenomenology associated with the CP-violating NMSSM Higgs sector will be performed in future works. We list a few possible directions at the end of the Conclusions.

We include in this calculation the important corrections to the Higgs spectrum in order to have more precise comparisons to current experimental limits: (i) full one-loop corrections to the Higgs-boson masses, and (ii) logarithmically enhanced two-loop corrections of order $\mathcal{O}(g_s^2 h^4)$ and $\mathcal{O}(h^6)$ with the renormalization-group (RG) improvement and minimization of the two-loop corrections. We also impose highly desirable conditions to limit the parameter space: (i) the LEP limits on the Higgs-boson mass and the chargino mass limit, (ii) the global minimum condition—the local minimum that we obtain is indeed the global minimum, and (iii) the positivity of the square of the Higgs-boson masses. We found that the RG-improved corrections have significant reduction in the allowed parameter space with respect to the LEP limits, the global minimum condition, and the positivity of the Higgs-mass squared.

Before we close this section let us list the parameters of this study. We have (i) the usual soft parameters in the MSSM: sfermion masses, A parameters, soft Higgs-boson masses, and $\tan\beta$; (ii) the additional parameters arisen in NMSSM: λ and κ in the superpotential, A_λ and A_κ in the soft-breaking sector, and the VEV v_S of the singlet Higgs field; (iii) the CP phases of A parameters, λ , κ , and the VEVs (but not all independent).

The organization of this paper is as follows. We write down the formalism in details in the next section, including minimization conditions, combinations of CP phases, tree-level mass matrices, and mixing between scalar and pseudoscalar Higgs bosons. In Sec. III, we calculate the full one-loop and logarithmically enhanced two-loop corrections using the RG-improved approach. Numerical presentation for a number of interesting scenarios will be demonstrated in Sec. IV, including comparisons to the previous results in literature where possible. We conclude and discuss our results in Sec. V.

2 Higgs sector at the tree level

2.1 Conventions

To begin with, we first introduce the NMSSM superpotential:

$$W_{\text{NMSSM}} = \widehat{U}^C \mathbf{h}_u \widehat{Q} \widehat{H}_u + \widehat{D}^C \mathbf{h}_d \widehat{H}_d \widehat{Q} + \widehat{E}^C \mathbf{h}_e \widehat{H}_d \widehat{L} + \lambda \widehat{S} \widehat{H}_u \widehat{H}_d + \frac{\kappa}{3} \widehat{S}^3, \quad (2.1)$$

where \widehat{S} denotes the singlet Higgs superfield, $\widehat{H}_{u,d}$ are the two $\text{SU}(2)_L$ doublet Higgs superfields, and \widehat{Q} , \widehat{L} and \widehat{U}^C , \widehat{D}^C , \widehat{E}^C are the matter doublet and singlet superfields, respectively, related to up- and down-type quarks and charged leptons. We note that, especially, the last cubic term with a dimensionless coupling κ respects an extra discrete Z_3 symmetry. The Yukawa couplings $\mathbf{h}_{u,d,e}$ are 3×3 complex matrices describing the quark and charged-lepton masses and mixing. In the expression, for example, the notation $\widehat{H}_u \widehat{H}_d \equiv \epsilon_{\alpha\beta} (\widehat{H}_u)^\alpha (\widehat{H}_d)^\beta$ is implicit. The superpotential leads to the tree-level Higgs potential, which is given by the sum

$$V_0 = V_F + V_D + V_{\text{soft}}, \quad (2.2)$$

where each term is given by

$$\begin{aligned} V_F &= |\lambda|^2 |S|^2 (H_d^\dagger H_d + H_u^\dagger H_u) + |\lambda H_u H_d + \kappa S^2|^2, \\ V_D &= \frac{g_2^2 + g_1^2}{8} (H_d^\dagger H_d - H_u^\dagger H_u)^2 + \frac{g_2^2}{2} (H_d^\dagger H_u) (H_u^\dagger H_d), \\ V_{\text{soft}} &= m_1^2 H_d^\dagger H_d + m_2^2 H_u^\dagger H_u + m_S^2 |S|^2 + \left(\lambda A_\lambda S H_u H_d - \frac{1}{3} \kappa A_\kappa S^3 + \text{h.c.} \right), \end{aligned} \quad (2.3)$$

with the gauge-coupling constants $g_1 = e/\cos\theta_W$ and $g_2 = e/\sin\theta_W$. Note the unusual minus(-) sign for the singlet soft-trilinear term proportional to A_κ^* .

Parametrizing the component fields of the two doublet and one singlet scalar Higgs fields and the VEVs as follows,

$$\begin{aligned} H_d &= \begin{pmatrix} \frac{1}{\sqrt{2}} (v_d + \phi_d^0 + ia_d) \\ \phi_d^- \end{pmatrix}, \\ H_u &= e^{i\theta} \begin{pmatrix} \phi_u^+ \\ \frac{1}{\sqrt{2}} (v_u + \phi_u^0 + ia_u) \end{pmatrix}, \\ S &= \frac{e^{i\varphi}}{\sqrt{2}} (v_S + \phi_S^0 + ia_S), \end{aligned} \quad (2.4)$$

*One can go back to the usual convention by taking $R_\kappa \rightarrow -R_\kappa$ or $\phi'_\kappa \rightarrow \phi'_\kappa + \pi$ in below.

we get the following tadpole conditions for the presumed vacuum:

$$\begin{aligned}
\frac{1}{v_d} \left\langle \frac{\partial V_0}{\partial \phi_d^0} \right\rangle &= m_1^2 + \frac{g_2^2 + g_1^2}{8} (v_d^2 - v_u^2) - R_\lambda \frac{v_u v_S}{v_d} + \frac{|\lambda|^2}{2} (v_u^2 + v_S^2) - \frac{1}{2} \mathcal{R} \frac{v_u v_S^2}{v_d} = 0, \\
\frac{1}{v_u} \left\langle \frac{\partial V_0}{\partial \phi_u^0} \right\rangle &= m_2^2 - \frac{g_2^2 + g_1^2}{8} (v_d^2 - v_u^2) - R_\lambda \frac{v_d v_S}{v_u} + \frac{|\lambda|^2}{2} (v_d^2 + v_S^2) - \frac{1}{2} \mathcal{R} \frac{v_d v_S^2}{v_u} = 0, \\
\frac{1}{v_S} \left\langle \frac{\partial V_0}{\partial \phi_S^0} \right\rangle &= m_S^2 - R_\lambda \frac{v_d v_u}{v_S} + \frac{|\lambda|^2}{2} (v_d^2 + v_u^2) + |\kappa|^2 v_S^2 - \mathcal{R} v_d v_u - R_\kappa v_S, \tag{2.5}
\end{aligned}$$

$$\begin{aligned}
\frac{1}{v_u} \left\langle \frac{\partial V_0}{\partial a_d} \right\rangle &= \frac{1}{v_d} \left\langle \frac{\partial V_0}{\partial a_u} \right\rangle = I_\lambda v_S + \frac{1}{2} \mathcal{I} v_S^2 = 0, \\
\frac{1}{v_S} \left\langle \frac{\partial V_0}{\partial a_S} \right\rangle &= I_\lambda \frac{v_d v_u}{v_S} - \mathcal{I} v_d v_u + I_\kappa v_S = 0, \tag{2.6}
\end{aligned}$$

where

$$\begin{aligned}
\mathcal{R} &= |\lambda| |\kappa| \cos(\phi'_\lambda - \phi'_\kappa), & \mathcal{I} &= |\lambda| |\kappa| \sin(\phi'_\lambda - \phi'_\kappa), \\
R_\lambda &= \frac{|\lambda| |A_\lambda|}{\sqrt{2}} \cos(\phi'_\lambda + \phi_{A_\lambda}), & R_\kappa &= \frac{|\kappa| |A_\kappa|}{\sqrt{2}} \cos(\phi'_\kappa + \phi_{A_\kappa}), \tag{2.7}
\end{aligned}$$

with

$$\phi'_\lambda \equiv \phi_\lambda + \theta + \varphi \quad \text{and} \quad \phi'_\kappa \equiv \phi_\kappa + 3\varphi. \tag{2.8}$$

The other parameters I_λ and I_κ can be reexpressed in terms of \mathcal{I} using the CP-odd tadpole conditions as

$$\begin{aligned}
I_\lambda &= \frac{|\lambda| |A_\lambda|}{\sqrt{2}} \sin(\phi'_\lambda + \phi_{A_\lambda}) = -\frac{1}{2} \mathcal{I} v_S, \\
I_\kappa &= \frac{|\kappa| |A_\kappa|}{\sqrt{2}} \sin(\phi'_\kappa + \phi_{A_\kappa}) = \frac{3}{2} \mathcal{I} \frac{v_d v_u}{v_S}. \tag{2.9}
\end{aligned}$$

Therefore, the only rephasing invariant physical CP phase at the tree level is $\phi'_\lambda - \phi'_\kappa$ and, once the absolute values of $|\lambda|$, $|\kappa|$, $|A_\lambda|$, and $|A_\kappa|$ are given, the other two combinations of CP phases, $\phi'_\lambda + \phi_{A_\lambda}$ and $\phi'_\kappa + \phi_{A_\kappa}$, can be determined up to a twofold ambiguity using the two CP-odd tadpole conditions in Eq. (2.6). We also observe that the soft masses m_1^2 , m_2^2 , and m_S^2 can be removed using the three CP-even tadpole conditions in Eq. (2.5).

From the potential, with the parametrization of the scalar Higgs fields as in Eq. (2.4), the scalar mass terms can be derived and they can be cast into the form

$$-\mathcal{L}_{\text{mass}} = M_{H^\pm}^{(0)2} H^+ H^- + \frac{1}{2} \Phi^T \mathcal{M}_N^{(0)2} \Phi \tag{2.10}$$

where $H^\pm = \phi_d^\pm \sin \beta + \phi_u^\pm \cos \beta$ with $\tan \beta = v_u/v_d$ and

$$\Phi^T \equiv (\phi_d^0, \phi_u^0, \phi_S^0, a, a_S) \tag{2.11}$$

with $a = a_d \sin \beta + a_u \cos \beta$, rotating away the zero mass Goldstone states. The tree-level charged Higgs-boson mass is given by

$$M_{H^\pm}^{(0)2} = M_W^2 + (2R_\lambda + \mathcal{R}v_S) \frac{v_S}{\sin 2\beta} - \frac{|\lambda|^2}{2} v^2. \quad (2.12)$$

The 5×5 symmetric mass matrix for the neutral Higgs boson is given by

$$\mathcal{M}_N^{(0)2} = \begin{pmatrix} \left(\mathcal{M}_S^{(0)2} \right)_{11} & \left(\mathcal{M}_S^{(0)2} \right)_{12} & \left(\mathcal{M}_S^{(0)2} \right)_{13} & 0 & -\frac{3}{2} \mathcal{I} v_u v_S \\ \left(\mathcal{M}_S^{(0)2} \right)_{21} & \left(\mathcal{M}_S^{(0)2} \right)_{22} & \left(\mathcal{M}_S^{(0)2} \right)_{23} & 0 & -\frac{3}{2} \mathcal{I} v_d v_S \\ \left(\mathcal{M}_S^{(0)2} \right)_{31} & \left(\mathcal{M}_S^{(0)2} \right)_{32} & \left(\mathcal{M}_S^{(0)2} \right)_{33} & \frac{1}{2} \mathcal{I} v v_S & 2 \mathcal{I} v_d v_u \\ 0 & 0 & \frac{1}{2} \mathcal{I} v v_S & (R_\lambda + \frac{1}{2} \mathcal{R} v_S) \frac{v^2 v_S}{v_d v_u} & (R_\lambda - \mathcal{R} v_S) v \\ -\frac{3}{2} \mathcal{I} v_u v_S & -\frac{3}{2} \mathcal{I} v_d v_S & 2 \mathcal{I} v_d v_u & (R_\lambda - \mathcal{R} v_S) v & R_\lambda \frac{v_d v_u}{v_S} + 2 \mathcal{R} v_d v_u + 3 R_\kappa v_S \end{pmatrix} \quad (2.13)$$

with

$$\begin{aligned} \left(\mathcal{M}_S^{(0)2} \right)_{11} &= \frac{g_2^2 + g_1^2}{4} v_d^2 + \left(R_\lambda + \frac{1}{2} \mathcal{R} v_S \right) \frac{v_u v_S}{v_d}, \\ \left(\mathcal{M}_S^{(0)2} \right)_{22} &= \frac{g_2^2 + g_1^2}{4} v_u^2 + \left(R_\lambda + \frac{1}{2} \mathcal{R} v_S \right) \frac{v_d v_S}{v_u}, \\ \left(\mathcal{M}_S^{(0)2} \right)_{33} &= R_\lambda \frac{v_d v_u}{v_S} + 2 |\kappa|^2 v_S^2 - R_\kappa v_S, \\ \left(\mathcal{M}_S^{(0)2} \right)_{12} &= \left(\mathcal{M}_S^{(0)2} \right)_{21} = \left(-\frac{g_2^2 + g_1^2}{4} + |\lambda|^2 \right) v_d v_u - \left(R_\lambda + \frac{1}{2} \mathcal{R} v_S \right) v_S, \\ \left(\mathcal{M}_S^{(0)2} \right)_{13} &= \left(\mathcal{M}_S^{(0)2} \right)_{31} = -R_\lambda v_u + |\lambda|^2 v_d v_S - \mathcal{R} v_u v_S, \\ \left(\mathcal{M}_S^{(0)2} \right)_{23} &= \left(\mathcal{M}_S^{(0)2} \right)_{32} = -R_\lambda v_d + |\lambda|^2 v_u v_S - \mathcal{R} v_d v_S. \end{aligned} \quad (2.14)$$

2.2 Mixing and mass spectrum with $\mathcal{I} \neq 0$

When $\mathcal{I} \neq 0$, we should consider the full 5×5 matrix (2.13) for the neutral Higgs-boson masses and mixing. In this case, the neutral Higgs bosons do not have to carry any definite CP parities and its mixing is described by the orthogonal 5×5 matrix $O_{\alpha i}$ as

$$(\phi_d^0, \phi_u^0, \phi_S^0, a, a_S)^T = O_{\alpha i} (H_1, H_2, H_3, H_4, H_5)^T \quad (2.15)$$

with $H_{1(5)}$ the lightest (heaviest) Higgs-mass eigenstate. Because of its CP-violating mixing, the couplings of the neutral Higgs bosons to the SM and SUSY particles are significantly modified. Among them the most eminent one is the couplings of the Higgs bosons to weak

gauge bosons in the interaction Lagrangian:

$$\mathcal{L}_{HVV} = g_2 M_W \left(W_\mu^+ W^{-\mu} + \frac{1}{2c_W^2} Z_\mu Z^\mu \right) \sum_i g_{H_iVV} H_i, \quad (2.16)$$

$$\mathcal{L}_{HHZ} = \frac{g_2}{4c_W} \sum_{i,j} g_{H_iH_jZ} Z^\mu (H_i \overleftrightarrow{\partial}_\mu H_j), \quad (2.17)$$

$$\mathcal{L}_{HH^\pm W^\mp} = -\frac{g_2}{2} \sum_i g_{H_iH^\pm W^\mp} W^{-\mu} (H_i i \overleftrightarrow{\partial}_\mu H^\pm) + \text{h.c.}, \quad (2.18)$$

where the couplings g_{H_iVV} , $g_{H_iH_jZ}$ and $g_{H_iH^\pm W^\mp}$ are given in terms of the neutral Higgs-boson mixing matrix O by

$$\begin{aligned} g_{H_iVV} &= c_\beta O_{1i} + s_\beta O_{2i}, \\ g_{H_iH_jZ} &= [(O_{4i}(c_\beta O_{2j} - s_\beta O_{1j}) - (i \leftrightarrow j))] \\ g_{H_iH^\pm W^\mp} &= c_\beta O_{2i} - s_\beta O_{1i} - iO_{4i}, \end{aligned} \quad (2.19)$$

leading to the following sum rules:

$$\begin{aligned} \sum_{i=1}^5 g_{H_iVV}^2 &= 1, \\ \sum_{i>j}^5 g_{H_iH_jZ}^2 &= 1, \\ g_{H_iVV}^2 + |g_{H_iH^\pm W^\mp}|^2 &= 1 - O_{3i}^2 - O_{5i}^2 \quad \text{for each } i. \end{aligned} \quad (2.20)$$

When the heavier two states have mass larger than that of the other three states, they effectively decouple from the mixing and the lighter three states tend to mix among themselves. To have a better understanding in this case we introduce the following basis:

$$\Phi' \equiv (\phi_H^0, a, \phi_h^0, \phi_S^0, a_S)^T = U \Phi = U (\phi_d^0, \phi_u^0, \phi_S^0, a, a_S)^T \quad (2.21)$$

with

$$U = \begin{pmatrix} -s_\beta & c_\beta & 0 & 0 & 0 \\ 0 & 0 & 0 & 1 & 0 \\ c_\beta & s_\beta & 0 & 0 & 0 \\ 0 & 0 & 1 & 0 & 0 \\ 0 & 0 & 0 & 0 & 1 \end{pmatrix}. \quad (2.22)$$

In the Φ' basis, the symmetric 5×5 mass matrix takes the form

$$(\mathcal{M}_N^{(0)2})' = U \mathcal{M}_N^{(0)2} U^T = \begin{pmatrix} \mathcal{M}_J^2 & \mathcal{M}_{JL}^2 \\ (\mathcal{M}_{JL}^2)^T & \mathcal{M}_L^2 \end{pmatrix}, \quad (2.23)$$

where

$$\mathcal{M}_J^2 = \begin{pmatrix} M_A^2 + \left(M_Z^2 - \frac{|\lambda|^2 v^2}{2}\right) s_{2\beta}^2 & 0 \\ 0 & M_A^2 \end{pmatrix}, \quad (2.24)$$

with

$$M_A^2 \equiv \frac{v_S}{\sin 2\beta} (2 R_\lambda + v_S \mathcal{R}). \quad (2.25)$$

Then, the tree-level charged Higgs-boson mass can be rewritten as

$$M_{H^\pm}^{(0)2} = M_W^2 + M_A^2 - \frac{|\lambda|^2}{2} v^2. \quad (2.26)$$

On the other hand, the 2×3 heavy-light mixing matrix is

$$\mathcal{M}_{JL}^2 = \begin{pmatrix} \left(-\frac{M_Z^2}{2} + \frac{|\lambda|^2 v^2}{4}\right) s_{4\beta} & -\frac{v}{4v_S} M_A^2 s_{4\beta} - \frac{vv_S}{2} \mathcal{R} c_{2\beta} & -\frac{3}{2} vv_S \mathcal{I} c_{2\beta} \\ 0 & \frac{1}{2} vv_S \mathcal{I} & \frac{v}{2v_S} M_A^2 s_{2\beta} - \frac{3vv_S}{2} \mathcal{R} \end{pmatrix}, \quad (2.27)$$

and the symmetric 3×3 mass matrix for the lighter states is given by

$$\mathcal{M}_L^2 = \begin{pmatrix} M_Z^2 c_{2\beta}^2 + \frac{1}{2} |\lambda|^2 v^2 s_{2\beta}^2 & vv_S \left[\left(|\lambda|^2 - \frac{M_A^2}{2v_S^2} s_{2\beta}^2 \right) - \frac{\mathcal{R}}{2} s_{2\beta} \right] & -\frac{3}{2} vv_S \mathcal{I} s_{2\beta} \\ & v^2 \left(\frac{M_A^2}{4v_S^2} s_{2\beta}^2 - \frac{\mathcal{R}}{4} s_{2\beta} \right) & v^2 \mathcal{I} s_{2\beta} \\ & +v_S^2 \left(2|\kappa|^2 - \frac{R_\kappa}{v_S} \right) & \\ & & \frac{v^2}{4v_S^2} M_A^2 s_{2\beta}^2 + \frac{3v^2}{4} \mathcal{R} s_{2\beta} \\ & & +3 R_\kappa v_S \end{pmatrix}. \quad (2.28)$$

We observe that, in the leading order, $\mathcal{M}_J^2 \sim M_A^2$, $\mathcal{M}_{JL}^2 \sim \epsilon M_A^2$, and $\mathcal{M}_L^2 \sim \epsilon^2 M_A^2$ with

$$\epsilon = \max \left(s_{2\beta}, \frac{v}{M_A}, \frac{v_S}{M_A}, \frac{R_\kappa}{M_A} \right). \quad (2.29)$$

In this case, the mass matrix $(\mathcal{M}_N^{(0)2})'$ could be systematically block diagonalized order by order in ϵ , as described in Appendix A. In the block-diagonalized basis, the symmetric heavier-state mass matrix becomes

$$\widetilde{\mathcal{M}}_J^2 = \begin{pmatrix} M_A^2 \left(1 + \frac{v^2}{4v_S^2} s_{2\beta}^2 \right) + \frac{v^2}{2} \mathcal{R} s_{2\beta} & v^2 \mathcal{I} s_{2\beta} \\ & M_A^2 \left(1 + \frac{v^2}{4v_S^2} s_{2\beta}^2 \right) - \frac{3v^2}{2} \mathcal{R} s_{2\beta} \end{pmatrix} + M_A^2 \cdot \mathcal{O}(\epsilon^4),$$

leading to two almost degenerate eigenmasses

$$M_{J_1, J_2}^2 \approx M_A^2 \left(1 + \frac{v^2}{4v_S^2} s_{2\beta}^2 \right) - v^2 s_{2\beta} \left(\mathcal{R}/2 \pm \sqrt{\mathcal{R}^2 + \mathcal{I}^2} \right) \quad (2.30)$$

and the mass splitting is of order $\mathcal{O}(\epsilon^3)$. On the other hand, by defining

$$Y \equiv M_A^2 s_{2\beta}^2 - 2|\lambda|^2 v_S^2, \quad (2.31)$$

one may obtain the following symmetric mass matrix for the lighter states

$$\widetilde{\mathcal{M}}_L^2 = \begin{pmatrix} M_Z^2 & -\frac{vY}{2v_S} - \frac{vv_S}{2} \mathcal{R} s_{2\beta} & -\frac{3vv_S}{2} \mathcal{I} s_{2\beta} \\ v_S^2 \left(2|\kappa|^2 - \frac{R_\kappa}{v_S} \right) - \frac{3v^2}{4} \mathcal{R} s_{2\beta} & 0 & \\ & & 3R_\kappa v_S + \frac{9v^2}{4} \mathcal{R} s_{2\beta} \end{pmatrix} + M_A^2 \cdot \mathcal{O}(\epsilon^4),$$

which gives rise to the eigenmasses

$$M_{L_{1,2}}^2 \approx \frac{1}{2} \left\{ \left[M_Z^2 + v_S^2 \left(2|\kappa|^2 - \frac{R_\kappa}{v_S} \right) - \frac{3}{4} v^2 s_{2\beta} \mathcal{R} \right] \pm \sqrt{\left[M_Z^2 - v_S^2 \left(2|\kappa|^2 - \frac{R_\kappa}{v_S} \right) + \frac{3}{4} v^2 s_{2\beta} \mathcal{R} \right]^2 + \left[\frac{v}{v_S} Y + vv_S s_{2\beta} \mathcal{R} \right]^2} \right\} \quad (2.32)$$

$$M_{L_3}^2 \approx 3R_\kappa v_S + \frac{9}{4} v^2 s_{2\beta} \mathcal{R}. \quad (2.33)$$

We note that the CP-mixing entries in the heavier-state matrix $\widetilde{\mathcal{M}}_J^2$ and the lighter matrix $\widetilde{\mathcal{M}}_L^2$ are proportional to the factors $v^2 \mathcal{I} s_{2\beta}$ or $vv_S \mathcal{I} s_{2\beta}$, respectively, and would not affect the approximated mass spectrum up to the order $O(\epsilon^2)$. This could be easily understood by observing the CP-mixing entries in \mathcal{M}_{JL}^2 (2.27) and \mathcal{M}_L^2 (2.28), which are proportional to \mathcal{I} , are suppressed by the factor ϵ^2 and ϵ^3 , respectively. In the CP-conserving limit or up to the order $O(\epsilon^2)$, our results agree with those in Ref. [26].

When the $U(1)$ PQ symmetry is not broken or $|\kappa| = \mathcal{R} = \mathcal{I} = R_\kappa/v_S = 0$, there is no CP-violating mixing and the determinant of the lower-right 2×2 submatrix of Eq. (2.13) for the CP-odd states vanishes, resulting in a massless CP-odd PQ axion; or else its mass is approximately given by Eq. (2.33). In the same PQ-symmetric limit, the lighter CP-even state becomes tachyonic unless $Y = 0$ as seen from Eq. (2.32). When the $U(1)$ PQ symmetry is broken, it is interesting to note that the condition $M_{L_1}^2 \geq 0$ gives

$$\left| M_A^2 s_{2\beta}^2 - 2|\lambda|^2 v_S^2 + v_S^2 s_{2\beta} \mathcal{R} \right| \leq \frac{2v_S M_Z}{v} \sqrt{2|\kappa|^2 v_S^2 - R_\kappa v_S - \frac{3}{4} \mathcal{R} v^2 s_{2\beta}}. \quad (2.34)$$

This, together with Eq. (2.25), leads to the following constraints on the parameter space

in the leading order:

$$\begin{aligned}
0 &\lesssim R_\kappa = \frac{|\kappa||A_\kappa|}{\sqrt{2}} \cos(\phi'_\kappa + \phi_{A_\kappa}) \lesssim 2 v_S |\kappa|^2, \\
M_{H^\pm}^{(0)} &\sim M_{J_1, J_2} \sim M_A \sim \frac{\sqrt{2} |\lambda| v_S}{s_{2\beta}}, \\
|A_\lambda| &\sim \frac{\sqrt{2} |\lambda| v_S}{s_{2\beta} \cos(\phi'_\lambda + \phi_{A_\lambda})} \sim \frac{M_A}{\cos(\phi'_\lambda + \phi_{A_\lambda})},
\end{aligned} \tag{2.35}$$

which more or less lift up the twofold ambiguity in using the two CP-odd tadpole conditions by fixing

$$\text{sign} [\cos(\phi'_\kappa + \phi_{A_\kappa})] = \text{sign} [\cos(\phi'_\lambda + \phi_{A_\lambda})] = +1. \tag{2.36}$$

2.3 Vacuum condition

Considering neutral fields only, the effective potential at tree level takes the form

$$\begin{aligned}
\tilde{V}_0(\tilde{\mathbf{v}}) &= \frac{1}{2} m_1^2 \tilde{v}_d^2 + \frac{1}{2} m_2^2 \tilde{v}_u^2 + \frac{1}{2} m_S^2 \tilde{v}_S^2 - R_\lambda \tilde{v}_d \tilde{v}_u \tilde{v}_S - \frac{1}{3} R_\kappa \tilde{v}_S^3 \\
&\quad + \frac{g_2^2 + g_1^2}{32} (\tilde{v}_d^2 - \tilde{v}_u^2)^2 + \frac{|\lambda|^2}{4} (\tilde{v}_d^2 \tilde{v}_u^2 + \tilde{v}_d^2 \tilde{v}_S^2 + \tilde{v}_u^2 \tilde{v}_S^2) \\
&\quad + \frac{|\kappa|^2}{4} \tilde{v}_S^4 - \frac{1}{2} \mathcal{R} \tilde{v}_d \tilde{v}_u \tilde{v}_S^2,
\end{aligned} \tag{2.37}$$

where $\tilde{\mathbf{v}} = (\tilde{v}_u, \tilde{v}_d, \tilde{v}_S, \tilde{\theta}, \tilde{\varphi})$ denotes the arbitrary constant fields. The CP phases of the VEVs enter into the potential through \mathcal{R} , R_λ , and R_κ under the CP-odd tadpole conditions. In the NMSSM, diverse vacua can exist. Following the classification discussed in Ref. [25], we define the following phases:

$$\begin{aligned}
\text{EW} &: v \neq 0, v_S \neq 0, \\
\text{I} &: v = 0, v_S \neq 0, \\
\text{II} &: v \neq 0, v_S = 0, \\
\text{SYM} &: v = v_S = 0,
\end{aligned} \tag{2.38}$$

where $v = \sqrt{v_d^2 + v_u^2}$. Unlike the MSSM at the tree level, the electroweak-broken vacuum (denoted by EW) is not necessarily the global minimum due to the presence of the cubic terms in the Higgs potential which are proportional to R_λ and R_κ . To ensure the presumed vacuum is the true global minimum of the potential, we require the vacuum energy for the chosen vacuum to be smaller than that for any other choices

$$V_0^{\text{EW}} \equiv \tilde{V}_0(\tilde{\mathbf{v}} = \mathbf{v}) < \tilde{V}_0(\tilde{\mathbf{v}} \neq \mathbf{v}). \tag{2.39}$$

After removing the soft masses $m_{1,2,S}^2$ using the CP-even tadpole conditions, the energy level of the EW vacuum can be rewritten as

$$\begin{aligned}
V_0^{\text{EW}} &= \frac{1}{8} v^2 \left\{ s_{2\beta}^2 \left[\left(\frac{2v_S R_\lambda + v_S^2 \mathcal{R}}{s_{2\beta}} \right) - \frac{|\lambda|^2 v^2}{2} \right] - 2|\lambda|^2 v_S^2 - M_Z^2 c_{2\beta}^2 \right\} \\
&+ \frac{\mathcal{R}}{8} v^2 v_S^2 s_{2\beta} - \frac{|\kappa|^2}{4} v_S^4 + \frac{R_\kappa}{6} v_S^3,
\end{aligned} \tag{2.40}$$

where $c_\beta = \cos \beta = v_d/v$ and $s_\beta = \sin \beta = v_u/v$. Here, as an example, we compare the vacuum energy of the phase EW with that of the phase II. The energy difference, which should be positive definite if the EW vacuum is the global minimum, is given by

$$\begin{aligned}
\Delta V_0^{\text{II-EW}} &\equiv V_0^{\text{II}} - V_0^{\text{EW}} \\
&= -\frac{1}{2} R_\lambda v_d v_u v_S - \frac{1}{6} R_\kappa v_S^3 - \frac{1}{2} \mathcal{R} v_d v_u v_S^2 + \frac{g_2^2 + g_1^2}{32} \{ (\bar{v}_d^2 - \bar{v}_u^2)^2 - (v_d^2 - v_u^2)^2 \} \\
&- \frac{|\lambda|^2}{4} \{ (\bar{v}_d^2 \bar{v}_u^2 - v_d^2 v_u^2) - v_d^2 v_S^2 - v_u^2 v_S^2 \} + \frac{|\kappa|^2}{4} v_S^4,
\end{aligned} \tag{2.41}$$

where V_0^{II} denotes the vacuum energy of the phase II with VEVs $\bar{\mathbf{v}} \equiv (\bar{v}_d, \bar{v}_u, 0, 0, 0)$. Since the two vacua $\bar{\mathbf{v}}$ and \mathbf{v} are the simultaneous solutions to the same tadpole conditions, the VEVs \bar{v}_d and \bar{v}_u are determined by the tadpole conditions taking $v_S = 0$ and using the same soft masses $m_{1,2,S}^2$ fixed by the EW vacuum. It should be noted that $\Delta V_0^{\text{II-EW}}$ can be negative if R_λ and/or R_κ with the positive signs become large, leading to a metastable EW vacuum. Comparison of the EW vacuum with the other vacua also gives similar expressions as Eq. (2.41). Therefore, the requirement for the global minimum can constrain the size of $|A_\lambda|$ and $|A_\kappa|$ [†].

3 Higgs sector at the one-loop level

The one-loop contributions to the Higgs-boson masses can be computed from the effective potential [27, 28]

$$V_1 = \frac{1}{64\pi^2} \text{Str} \left[\mathcal{M}^4 \left(\log \frac{\mathcal{M}^2}{Q_0^2} - \frac{3}{2} \right) \right] \tag{3.1}$$

where Q_0 is the renormalization scale and \mathcal{M} is the field-dependent mass matrix of all modes that couple to the Higgs bosons. The supertrace is defined as $\text{Str}[f(\mathcal{M}^2)] \equiv \sum_i C_i (-1)^{2s_i} (2s_i + 1) [f(m_i^2)]$, where C_i is the color degrees of freedom and s_i is the spin of the i^{th} particle. The field-dependent third-generation quark masses are given by

$$m_b^2 = |h_b|^2 |H_d^0|^2; \quad m_t^2 = |h_t|^2 |H_u^0|^2, \tag{3.2}$$

[†] Although a sufficiently long-lived metastable vacuum may be viable, we will not consider such a case in this work.

where $H_{d,u}^0$ are the neutral components of $H_{d,u}$. The corresponding eigenvalues of the squark mass matrices are

$$\begin{aligned}
m_{\tilde{t}_{1,2}}^2 &= \frac{1}{2} \left[M_{\tilde{Q}}^2 + M_{\tilde{U}}^2 + 2|h_t|^2 |H_u^0|^2 + \frac{g_2^2 + g_1^2}{4} (|H_d^0|^2 - |H_u^0|^2) \right. \\
&\quad \left. \pm \sqrt{\left[M_{\tilde{Q}}^2 - M_{\tilde{U}}^2 + x_t (|H_d^0|^2 - |H_u^0|^2) \right]^2 + 4|h_t|^2 |A_t H_u^0 - \lambda^* S^*(H_d^0)^*|^2} \right], \\
m_{\tilde{b}_{1,2}}^2 &= \frac{1}{2} \left[M_{\tilde{Q}}^2 + M_{\tilde{D}}^2 + 2|h_b|^2 |H_d^0|^2 - \frac{g_2^2 + g_1^2}{4} (|H_d^0|^2 - |H_u^0|^2) \right. \\
&\quad \left. \pm \sqrt{\left[M_{\tilde{Q}}^2 - M_{\tilde{D}}^2 - x_b (|H_d^0|^2 - |H_u^0|^2) \right]^2 + 4|h_b|^2 |A_b H_d^0 - \lambda^* S^*(H_u^0)^*|^2} \right], \quad (3.3)
\end{aligned}$$

where

$$x_t = \frac{1}{4} \left(g_2^2 - \frac{5}{3} g_1^2 \right) \quad \text{and} \quad x_b = \frac{1}{4} \left(g_2^2 - \frac{1}{3} g_1^2 \right). \quad (3.4)$$

In Eq. (3.3), $M_{\tilde{Q}}^2$, $M_{\tilde{U}}^2$, and $M_{\tilde{D}}^2$ are real soft-SUSY breaking parameters and A_t and A_b are complex soft-SUSY breaking parameters, $A_q = |A_q| e^{i\phi_{A_q}}$ with $q = t, b$. For the explicit expressions of the corrections to the Higgs-boson mass matrix, we refer to Ref. [29] [‡].

While the relation between I_κ and \mathcal{I} remains the same as in Eq. (2.9), the tree-level relation between I_λ and \mathcal{I} is modified in the presence of the one-loop corrections as

$$I_\lambda = \frac{|\lambda| |A_\lambda|}{\sqrt{2}} \sin(\phi'_\lambda + \phi_{A_\lambda}) = -\frac{1}{2} \mathcal{I} v_S - \Delta I_\lambda, \quad (3.5)$$

where

$$\Delta I_\lambda = \frac{3}{16\pi^2} \sum_{q=t,b} |h_q|^2 I_q f(\langle m_{\tilde{q}_1}^2 \rangle, \langle m_{\tilde{q}_2}^2 \rangle) \quad (3.6)$$

with

$$I_q = \frac{|\lambda| |A_q|}{\sqrt{2}} \sin(\phi'_\lambda + \phi_{A_q}) \quad (3.7)$$

and

$$f(a, b) = \frac{1}{a-b} \left[a \left(\log \frac{a}{Q_0^2} - 1 \right) - b \left(\log \frac{b}{Q_0^2} - 1 \right) \right]. \quad (3.8)$$

The one-loop corrected charged Higgs-boson mass is given by

$$M_{H^\pm}^2 = M_{H^\pm}^{(0)2} + \Delta M_{H^\pm}^2 \quad (3.9)$$

where we refer to Ref. [30] for the explicit form of the correction $\Delta M_{H^\pm}^2$.

In this work, we have included logarithmically enhanced two-loop corrections of the order $\mathcal{O}(g_s^2 h^4)$ and $\mathcal{O}(h^6)$, where g_s is the strong gauge coupling. We have adopted the

[‡]In addition to the dominant contribution from third-generation quarks and squarks, we have included contributions from the weak gauge bosons in our numerical analysis.

algorithm suggested in Ref. [31], which incorporates the effects of the RG improvement and minimizes the two-loop corrections. Including the full one-loop radiative corrections, the 5×5 mass matrix of the neutral Higgs boson can be denoted by

$$\mathcal{M}_N^2 = \mathcal{M}_N^{(0)2} + \Delta\mathcal{M}_N^2 \quad (3.10)$$

where the one-loop correction part may further be decomposed into

$$\Delta\mathcal{M}_N^2 = (\Delta\mathcal{M}_N^2)_{\text{LL}} + (\Delta\mathcal{M}_N^2)_{\text{mix}}. \quad (3.11)$$

The first term contains the genuine logarithmic contributions which are present even when the left-right mixing of the third-generation squarks is absent. The second term describes the threshold effects arising from the mass splittings due to the left-right mixing in the third-generation squark sectors. The RG-improved mass matrix can be well approximated by replacing m_t and m_b in each term by the running masses at appropriate scales as in

$$\begin{aligned} (\Delta\mathcal{M}_N^2)_{\text{RG}} &\simeq \overline{(\Delta\mathcal{M}_N^2)_{\text{LL}}} + \overline{(\Delta\mathcal{M}_N^2)_{\text{mix}}} \\ &\equiv (\Delta\mathcal{M}_N^2)_{\text{LL}}[m_t(\mu_t), m_b(\mu_b)] + (\Delta\mathcal{M}_N^2)_{\text{mix}}[m_t(\mu_{\tilde{t}}), m_b(\mu_{\tilde{b}})] \end{aligned} \quad (3.12)$$

where the intermediate scales $\mu_{\tilde{t}}^2 = m_t \mu_{\tilde{t}}$ and $\mu_{\tilde{b}}^2 = m_b \mu_{\tilde{b}}$ with

$$\begin{aligned} \mu_{\tilde{t}}^2 &= \max(M_{\tilde{Q}}^2 + m_t^2, M_{\tilde{U}}^2 + m_t^2), \\ \mu_{\tilde{b}}^2 &= \max(M_{\tilde{Q}}^2 + m_b^2, M_{\tilde{D}}^2 + m_b^2). \end{aligned} \quad (3.13)$$

To obtain the quark masses at the SUSY and intermediate scales, we used the RG equations (RGEs) of the two-Higgs doublet model

$$\begin{aligned} \frac{d m_b^2}{d \ln \mu^2} &= \frac{1}{64\pi^2} [6h_b^2 + 2h_t^2 - 32g_s^2] m_b^2, \\ \frac{d m_t^2}{d \ln \mu^2} &= \frac{1}{64\pi^2} [6h_t^2 + 2h_b^2 - 32g_s^2] m_t^2, \end{aligned} \quad (3.14)$$

when $\mu > M_A$ assuming $M_A < \max(\mu_{\tilde{t}}, \mu_{\tilde{b}})$. When $\mu \leq M_A$, the SM RGEs are used:

$$\begin{aligned} \frac{d m_b^2}{d \ln \mu^2} &= \frac{1}{64\pi^2} [6(h_b^{\text{SM}})^2 - 6(h_t^{\text{SM}})^2 - 32g_s^2] m_b^2, \\ \frac{d m_t^2}{d \ln \mu^2} &= \frac{1}{64\pi^2} [6(h_t^{\text{SM}})^2 - 6(h_b^{\text{SM}})^2 - 32g_s^2] m_t^2. \end{aligned} \quad (3.15)$$

4 Numerical analysis

In this section, we present the numerical results of the RG-improved calculation of the masses and mixing matrix of the NMSSM Higgs bosons in the presence of nontrivial CP

phases. We make comparisons, where possible, with other RG-improved calculations without CP phases [32] and the one-loop calculations including CP phases but without the RG improvement [29]. The input parameters for the Higgs sector in our numerical study are specified as follows:

$$\begin{aligned}
\text{tree level} & : |\lambda|, |\kappa|, \tan\beta; |A_\lambda|, |A_\kappa|, v_S \\
\text{1-loop level} & : M_{\tilde{Q}}, M_{\tilde{U}}, M_{\tilde{D}}, |A_t|, |A_b| \\
\text{CP phases} & : \phi'_\lambda, \phi'_\kappa; \phi_{A_t}, \phi_{A_b} \\
\text{signs of} & : \cos(\phi'_\lambda + \phi_{A_\lambda}), \cos(\phi'_\kappa + \phi_{A_\kappa}).
\end{aligned} \tag{4.1}$$

For the renormalization scale Q_0 we take the top-quark mass as in Refs. [17, 19, 33].

On the scenarios under consideration in this section, we have imposed the following three conditions:

- the LEP limits [24],
- the global minimum condition requiring that the electroweak vacuum chosen by fixing the values of $\tan\beta$ and v_S is the global minimum of the RG-improved effective potential, and
- the positiveness of the Higgs masses squared, $M_H^2 > 0$, abandoning the parameter space in which one or more of the Higgs states become tachyonic.

In order to determine whether the prescribed EW vacuum is the global minimum or not, we minimize the effective potential numerically. First, the tadpole conditions are solved for input VEVs \mathbf{v}_{in} and then the solution is fed into the potential. Then the potential is numerically minimized in the range $(v_d, v_u|c_\theta|, v_u|s_\theta|, v_S|c_\varphi|, v_S|s_\varphi|) < 10$ TeV using the downhill simplex (Nelder-Mead) method [34]. The output minimum is denoted by \mathbf{v}_{out} . In the acceptable cases, the numerically obtained \mathbf{v}_{out} is exactly the same as the input \mathbf{v}_{in} up to the Z_3 symmetry. Depending on the parameter space, however, some \mathbf{v}_{out} may exist such that $V_{\text{eff}}(\mathbf{v}_{\text{out}}) < V_{\text{eff}}(\mathbf{v}_{\text{in}})$. In most cases, $\mathbf{v}_{\text{out}} (\neq \mathbf{v}_{\text{in}})$ corresponds to the VEVs in one of the three phases I, II, or SYM (2.38) in which one or both v and v_S are vanishing. When \mathbf{v}_{out} has $v_{u,d} \neq 0$ and $v_S \neq 0$ but with $v_{\text{out}} \neq 246$ GeV, it can be made acceptable in principle by rescaling the Higgs VEVs to make $v_{\text{out}} = 246$ GeV. But the rescaling may require compensating changes of the original values of $\tan\beta$ and v_S to satisfy the tadpole conditions. In this work, we discard such cases by keeping $\tan\beta$ and v_S fixed.

Before we go into various scenarios we offer a comment about the range of $\tan\beta$. It has been shown in Ref. [29] and we have also verified that large $\tan\beta > 20$ GeV is not favored by the LEP and global minimum constraints. Furthermore, the CP-violating scalar-pseudoscalar mixing is suppressed by large $\tan\beta$. We therefore employ a small to moderate $\tan\beta$ in the following scenarios.

4.1 A typical scenario

We first consider a typical scenario in which the heavier Higgs bosons are relatively light by choosing a small $\tan\beta$ and a moderate v_S [26]:

$$\begin{aligned} \tan\beta &= 3, \quad v_S = 750 \text{ GeV}, \\ M_{\tilde{Q}} &= M_{\tilde{U}} = M_{\tilde{D}} = |A_t| = |A_b| = 1000 \text{ GeV}, \\ \phi'_\lambda &= 0, \quad \phi_{A_t} = \phi_{A_b} = 0, \\ \text{sign}[\cos(\phi'_\kappa + \phi_{A_\kappa})] &= \text{sign}[\cos(\phi'_\lambda + \phi_{A_\lambda})] = +1, \end{aligned} \quad (4.2)$$

while varying

$$|\lambda|, |\kappa|; \quad |A_\lambda|, |A_\kappa|; \quad \phi'_\kappa. \quad (4.3)$$

For definiteness we have fixed $M_1 = M_2 = -200 \text{ GeV}$.

In Fig. 1, we show the allowed region satisfying the three conditions in the $|\kappa|$ - $|\lambda|$ plane when $|A_\lambda| = 500 \text{ GeV}$ and $|A_\kappa| = 100 \text{ GeV}$ for three values of the tree-level CP phase: $\phi'_\kappa = 0^\circ$ (upper panel), 90° (lower left panel), and 180° (lower right panel).

The magenta, blue, and red lines denote the LEP limits, the global minimum condition, and the positiveness of the Higgs mass squared, respectively. The solid (dotted) lines are after (before) the inclusion of the RG improvement. The vertical solid line denotes the chargino mass limit, $m_{\tilde{\chi}^\pm} > 104 \text{ GeV}$ [35]. For $\phi'_\kappa = 0^\circ$, we observe that the LEP constraint is significantly strengthened by the RG improvement, allowing only relatively large couplings with $|\lambda| \gtrsim 0.45$ and $|\kappa| \gtrsim 0.22$. In this regard, the parameter space point of $|\lambda| = 0.3$ and $|\kappa| = 0.1$ considered in Ref. [26], which is marginally compatible with the LEP limits without the RG improvement, is completely ruled out with the inclusion of the RG improvement. For the condition of $M_H^2 > 0$, we see that too large $|\lambda|$ is not allowed when $|\kappa| \lesssim 0.5$. This can be understood from Eq. (2.32) by observing that due to the third negative term in the first line and the second term inside the square root below, the lighter state mass $M_{L_1}^2$ could become negative when $|\lambda|$ is too large, unless the term $2|\kappa|^2 v_S^2$ in the first line is large enough. Nevertheless, after imposing the current LEP bounds, we see that the condition does not rule out more regions in the $|\kappa|$ - $|\lambda|$ plane. On the other hand, we see that the global minimum condition is always stronger than the $M_H^2 > 0$ condition and it is more restrictive than the LEP bounds in the region $0.55 \lesssim |\kappa| \lesssim 0.7$ when $|\lambda| \gtrsim 0.9$. For $\phi'_\kappa = 90^\circ$, the theoretically allowed region is significantly reduced and no region remains after applying the LEP limits. For $\phi'_\kappa = 180^\circ$, we still see no region compatible with the LEP bounds after the inclusion of the RG improvement.

In Fig. 2, we show the allowed region in the $|A_\kappa|$ - $|A_\lambda|$ plane for the three values of $\phi'_\kappa = 0^\circ, 90^\circ$, and 180° . We have taken $|\lambda| = 0.3$ and $|\kappa| = 0.1$ for comparisons with the results presented in [26], though this point has been ruled out by the LEP limits taking into account the RG improvement. Note that we only show the LEP limits without the

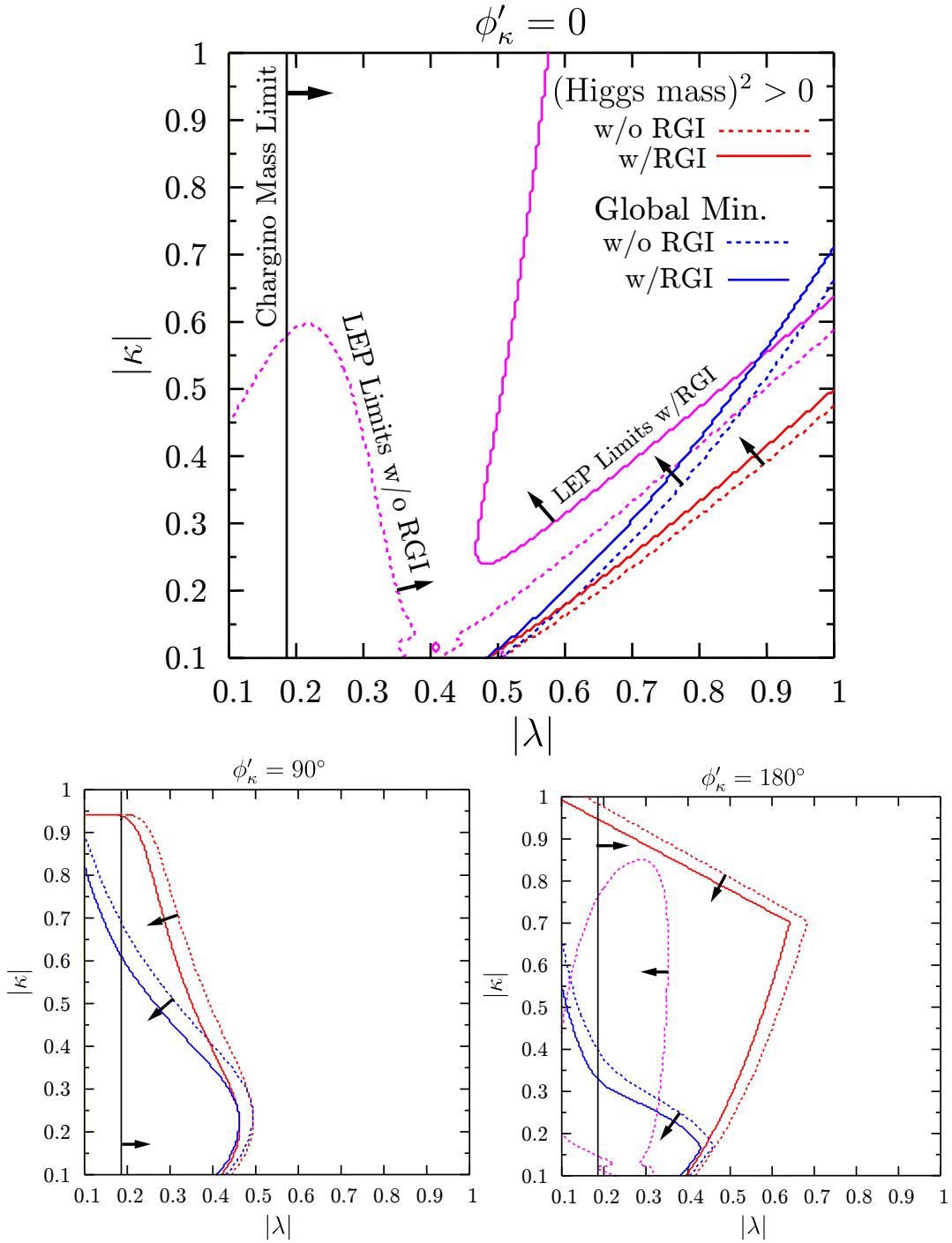


Figure 1: The allowed region in the $|\kappa|$ - $|\lambda|$ plane for the scenario in Eq. (4.2) with $|A_\lambda| = 500$ GeV and $|A_\kappa| = 100$ GeV for three values of $\phi'_\kappa = 0^\circ$ (upper panel), $\phi'_\kappa = 90^\circ$ (lower left panel), and $\phi'_\kappa = 180^\circ$ (lower right panel). RGI stands for the RG improvement.

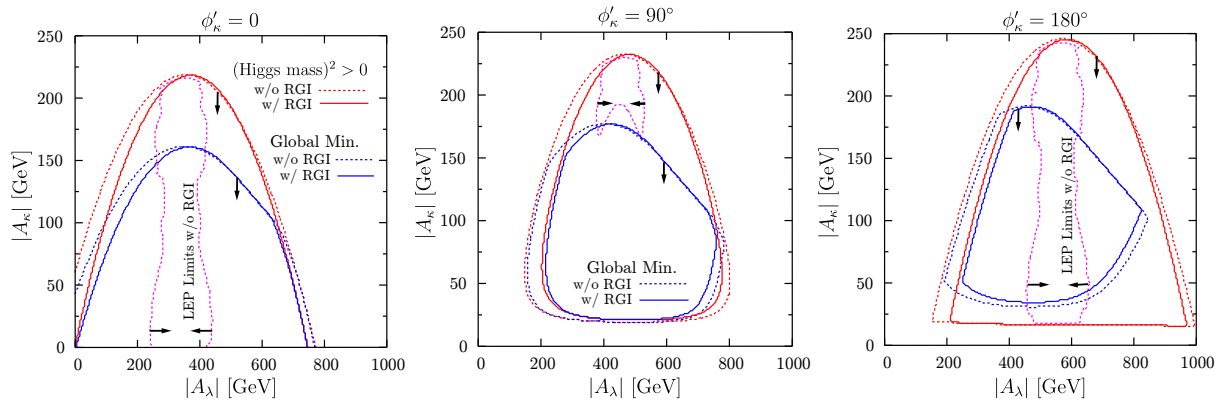


Figure 2: The allowed region in the $|A_\kappa|$ - $|A_\lambda|$ plane for the three values of $\phi'_\kappa = 0^\circ$ (left panel), 90° (middle panel), and 180° (right panel). The scenario in Eq. (4.2) is taken with $|\lambda| = 0.3$ and $|\kappa| = 0.1$. The lines are the same as in Fig. 1.

RG improvement here. By changing ϕ'_κ from 0° to 180° , we observe that the allowed region moves to the direction of increasing $|A_\lambda|$ and $|A_\kappa|$. Specifically, $|A_{\kappa,\lambda}| = 0$ GeV is not allowed when $\phi'_\kappa > 0^\circ$ due to the CP-odd tadpole conditions with $\mathcal{I} \neq 0$; see Eq. (2.9). We also observe that the allowed region is very small when CP is maximally violated with $\phi'_\kappa = 90^\circ$; see the middle frame. This implies that the inclusion of the CP phases may change the phenomenological features of the Higgs sector significantly together with the RG improvement. We pursue this issue further in the next section with a scenario compatible with the LEP limits. Otherwise, a similar discussion can be applied as in Fig. 1: (i) the global minimum condition is always stronger than the $M_H^2 > 0$ condition and (ii) it further constrains the parameter space in addition to the LEP limits.

The left plot in Fig. 3 shows the numerically obtained VEVs (\mathbf{v}_{out}) as a function of $|A_\kappa|$ taking $\phi'_\kappa = 0$ and $|A_\lambda| = 500$ GeV with $|\lambda| = 0.3$ and $|\kappa| = 0.1$. In the region, $0 \leq |A_\kappa| \lesssim 141$ GeV, the prescribed VEVs $\mathbf{v}_{\text{EW}} = \mathbf{v}_{\text{in}} = (v_d = 78 \text{ GeV}, v_u = 234 \text{ GeV}, v_S = 750 \text{ GeV})$ agree with \mathbf{v}_{out} and thus satisfy the global minimum condition. For $|A_\kappa| \gtrsim 141$ GeV, however, the global minimum moves to phase II with $\mathbf{v}_{\text{II}} = (v_d = 0 \text{ GeV}, v_u = 50 \text{ GeV}, v_S = 0 \text{ GeV})$. The energy levels of the two vacua are plotted in the middle panel. The EW vacuum energy ($V_{\text{eff}}(\mathbf{v}_{\text{in}})$) becomes larger as $|A_\kappa|$ increases. The linear dependence is coined from the R_κ term appearing in the potential at tree level, see Eq. (2.40), with no $|A_\kappa|$ -dependent terms in the one-loop effective potential. On the other hand, the vacuum energy of phase II $V_0^{\text{II}} = -(g_2^2 + g_1^2)v_u^4/32 + (\text{one-loop corrections}) \sim -3 \times 10^5 \text{ GeV}^4$ is independent of $|A_\kappa|$ as shown in the figure. In the right panel, for a given value of $|A_\kappa|$ the effective potential is plotted along the direction which connects the two vacua $\mathbf{v}_{\text{II}} = (v_d = 0 \text{ GeV}, v_u = 50 \text{ GeV}, v_S = 0 \text{ GeV})$ and $\mathbf{v}_{\text{EW}} = (v_d = 78 \text{ GeV},$

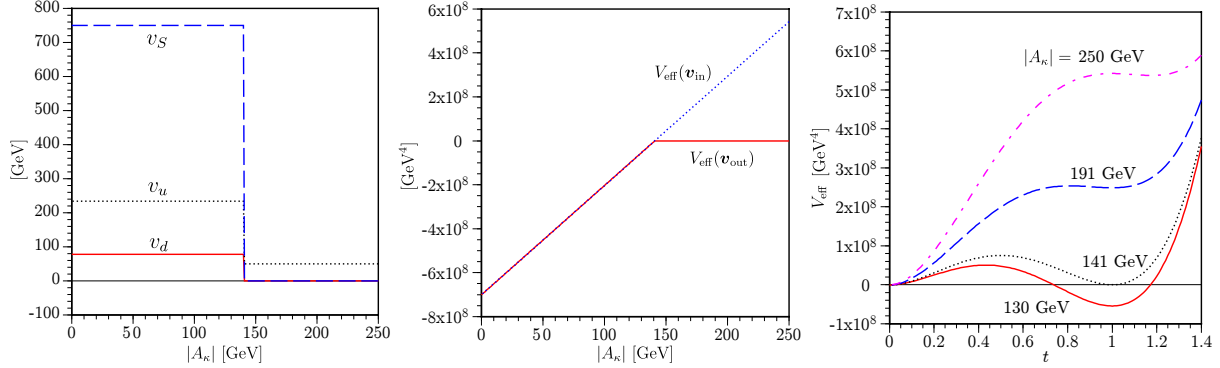


Figure 3: The output VEVs v_u , v_d , and v_S as functions of $|A_\kappa|$ (left panel) for the scenario in Eq. (4.2) taking $|\lambda| = 0.3$, $|\kappa| = 0.1$, $|A_\lambda| = 500$ GeV, and $\phi'_\kappa = 0$. The middle panel shows the vacuum energies for the input and output vacua as functions of $|A_\kappa|$, which separates from each other when $|A_\kappa|$ is larger than 141 GeV. In the right panel, the vacuum energies along the direction connecting the II ($t = 0$) and EW ($t = 1$) vacua are shown for several values of $|A_\kappa|$.

$v_u = 234$ GeV, $v_S = 750$ GeV). The direction is parametrized by t such that

$$\mathbf{v} = (\mathbf{v}_{\text{EW}} - \mathbf{v}_{\text{II}})t + \mathbf{v}_{\text{II}}, \quad (4.4)$$

and we are moving from the first minimum (\mathbf{v}_{II}) to the second extremum (\mathbf{v}_{EW}) as the parameter t increases from 0 to 1. We note that the EW vacuum is the global minimum when $|A_\kappa| = 130$ GeV (or $|A_\kappa| < 141$ GeV) and it becomes degenerate with the phase II vacuum when $|A_\kappa| \simeq 141$ GeV. If $|A_\kappa|$ increases further, the EW vacuum is destabilized or $M_H^2 < 0$ when $|A_\kappa| \simeq 191$ GeV and beyond the point, it turns into the maximum as shown by the line with $|A_\kappa| = 250$ GeV.

Before moving to the next scenario, we examine the renormalization scale (Q_0) dependence of the Higgs-mass spectrum. In Fig. 4, we show the masses of the lower three (left panel) and the heavier two (right panel) neutral Higgs states in the range between $Q_0 = 100$ GeV to 1000 GeV. We consider the CP-conserving case with $\phi'_\kappa = 0$ taking $|\lambda| = 0.3$, $|\kappa| = 0.1$, $|A_\lambda| = 500$ GeV, and $|A_\kappa| = 100$ GeV. First of all, we observe that the implementation of the RG improvement decreases the Q_0 dependence of the masses. The heavier states show the larger variation in their masses than the lighter ones. Among the lighter states the singlet CP-odd state H_3 is hardly affected by the loop corrections due the small value of $|\kappa| = 0.1$ and the H_1 state is less affected by the RG improvement than H_2 but shows stronger dependence on Q_0 . We find similar behaviors in the results obtained by using the NMHDECAY code [32]. In the CP-conserving limit, the NMHDECAY results are in agreement with ours after taking into account the Q_0 dependence and subleading contributions ignored in our calculation.

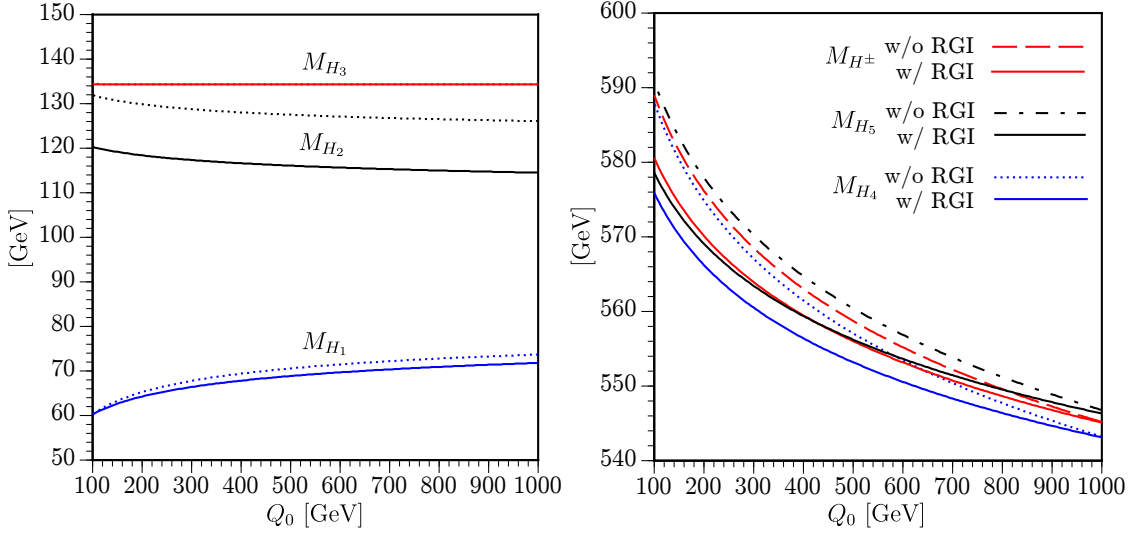


Figure 4: The light (left panel) and heavy (right panel) Higgs boson masses as functions of the renormalization scale Q_0 for the scenario in Eq. (4.2) taking $|\lambda| = 0.3$, $|\kappa| = 0.1$, $|A_\lambda| = 500$ GeV, $|A_\kappa| = 100$ GeV, and $\phi'_\kappa = 0$, with (solid lines) and without (dashed lines) RGI.

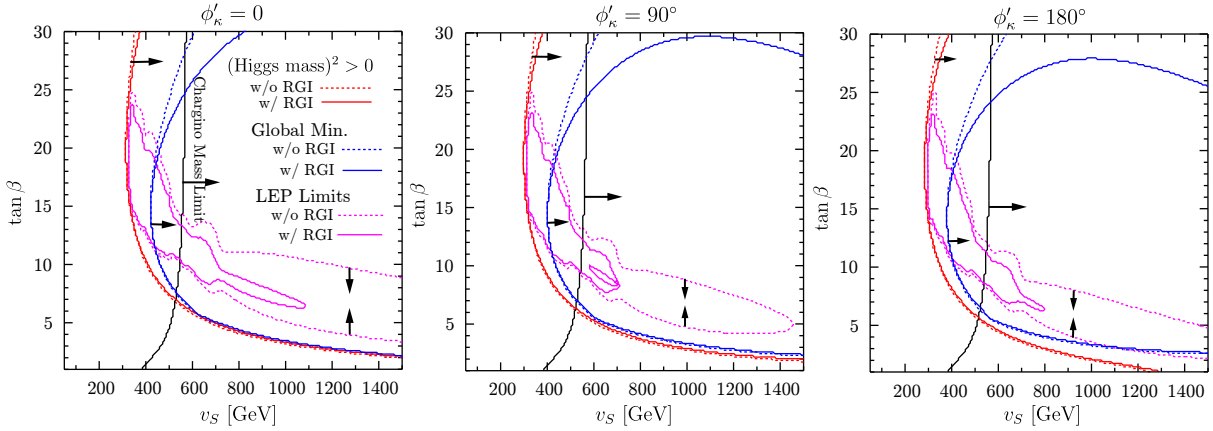


Figure 5: The allowed region in the $\tan\beta$ - v_S plane for the three values of $\phi'_\kappa = 0^\circ$ (left panel), 90° (middle panel), and 180° (right panel). We have taken $|\lambda| = 0.3$, $|\kappa| = 0.15$, $|A_\lambda| = 1200$ GeV, and $|A_\kappa| = 130$ GeV with $M_{\tilde{Q}} = M_{\tilde{U}} = M_{\tilde{D}} = |A_t| = |A_b| = 1000$ GeV, $\phi'_\lambda = \phi_{A_t} = \phi_{A_b} = 0$, $M_1 = M_2 = -200$ GeV, and $\text{sign}[\cos(\phi'_\kappa + \phi_{A_\kappa})] = \text{sign}[\cos(\phi'_\lambda + \phi_{A_\lambda})] = +1$.

4.2 A LEP-compatible scenario

The scenario considered in the previous section is not compatible with the LEP limits after taking into account the RG improvement. Moreover, we observe that the LEP limits

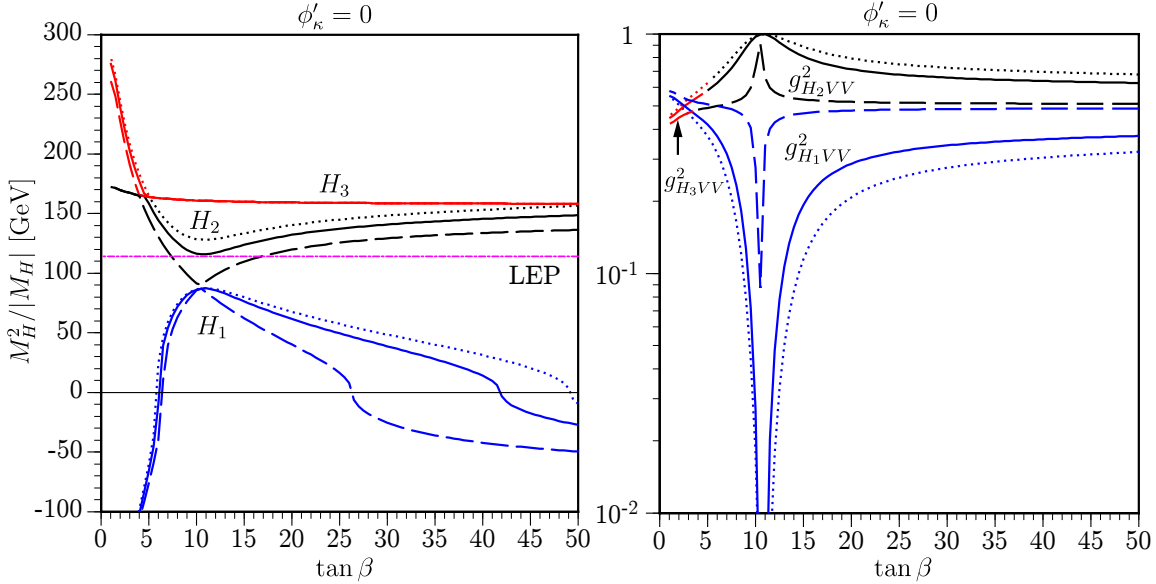


Figure 6: The masses $M_{H_i}^2/|M_{H_i}|$ (left panel) and couplings $g_{H_i V V}^2$ (right panel) as functions of $\tan\beta$. The dashed lines are at the tree level and the dotted and solid lines at the one-loop level without and with the RGI, respectively. We fix $v_S = 600$ GeV while other parameters are the same as in Fig. 5.

become very strong with nontrivial CP phases. In this section, we move to a higher value of $\tan\beta$ toward a LEP-compatible scenario independently of CP phases.

In Fig. 5, we show the allowed region in the $\tan\beta$ - v_S plane for the three values of $\phi'_\kappa = 0^\circ$ (left panel), 90° (middle panel), and 180° (right panel). We observe that $\tan\beta$ is bounded above by ~ 18 due to the LEP and global minimum constraints and further we have $\tan\beta \lesssim 13$ by applying the chargino mass limit. We note the upper limit on $\tan\beta$ is almost independent of ϕ'_κ . In Fig. 6 we show the masses $M_{H_i}^2/|M_{H_i}|$ (left panel) and couplings $g_{H_i V V}^2$ (right panel) for the lighter three states as functions of $\tan\beta$ while fixing $v_S = 600$ GeV. The mass of H_2 is always above the SM LEP limit while M_{H_1} is below it. For $\tan\beta \gtrsim 5$ where $M_{H_1}^2 > 0$, we find that $H_3 \sim a_S$ and H_1 and H_2 are mixtures mostly of ϕ_u and ϕ_S [§]. We find that the mass difference between the two lightest states becomes the smallest when $\tan\beta \sim 10$ and H_1 becomes dominated by the singlet component there, explaining why the coupling $g_{H_1 V V}$ almost vanishes; see the right frame. The $\tan\beta$ value at which the resonance occurs could be inferred from Eq. (2.32) by requiring $Y = 0$ [¶] or $\tan\beta \sim \sqrt{2}|A_\lambda|/|\lambda|v_S \sim 10$. As $\tan\beta$ grows, M_{H_1} decreases and the size of the coupling $g_{H_1 V V}$ increases, leading us to the fact that the large value of $\tan\beta$ is not compatible with the LEP limits.

[§] The heavier neutral states are such as $H_4 \sim a$ and $H_5 \sim \phi_d$.

[¶] We note $M_Z^2 \simeq v_S^2 (2|\kappa|^2 - R_\kappa/v_S)$ for the parameters chosen.

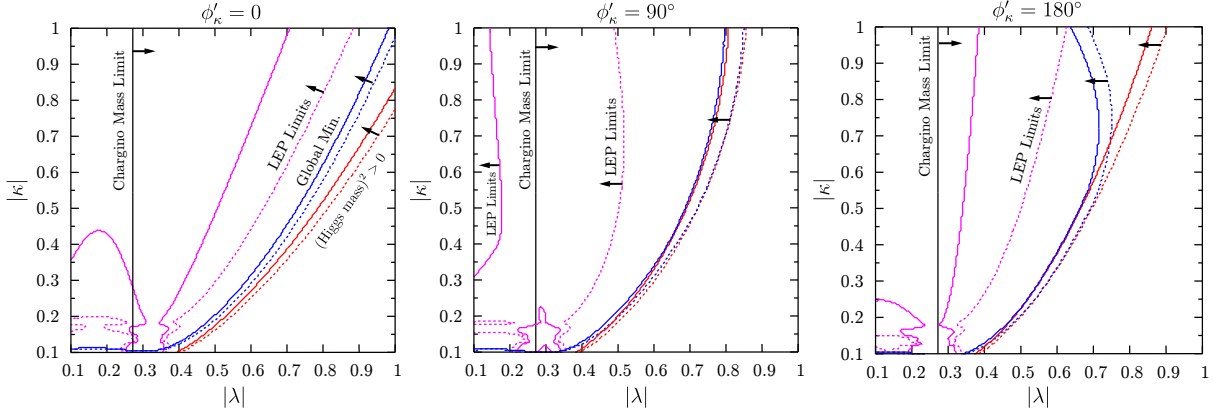


Figure 7: The allowed region in the $|\kappa|$ - $|\lambda|$ plane for the scenario in Eq. (4.5) with $|A_\lambda| = 1200$ GeV and $|A_\kappa| = 130$ GeV for the three values of $\phi'_\kappa = 0^\circ, 90^\circ$, and 180° . The lines are the same as in Fig. 1.

Combining these observations, we have fixed the parameters of our LEP-compatible scenario as

$$\begin{aligned}
\tan \beta &= 10, \quad v_S = 600 \text{ GeV}, \\
M_{\tilde{Q}} &= M_{\tilde{U}} = M_{\tilde{D}} = |A_t| = |A_b| = 1000 \text{ GeV}, \\
\phi'_\lambda &= 0, \quad \phi_{A_t} = \phi_{A_b} = 0, \\
\text{sign} [\cos(\phi'_\kappa + \phi_{A_\kappa})] &= \text{sign} [\cos(\phi'_\lambda + \phi_{A_\lambda})] = +1,
\end{aligned} \tag{4.5}$$

varying, again,

$$|\lambda|, |\kappa|; |A_\lambda|, |A_\kappa|; \phi'_\kappa. \tag{4.6}$$

We have fixed $M_1 = M_2 = -200$ GeV as in the previous case. We observe that the effects of the CP phases ϕ_{A_t} and ϕ_{A_b} are negligible in this scenario and we simply take $\phi_{A_t} = \phi_{A_b} = 0$.

In Fig. 7, we show the allowed region in the $|\kappa|$ - $|\lambda|$ plane taking $|A_\lambda| = 1200$ GeV and $|A_\kappa| = 130$ GeV for the three values of $\phi'_\kappa = 0^\circ, 90^\circ$, and 180° . We again see that the LEP limits, the global minimum, and the positive M_H^2 conditions become stronger with the RG improvement. Among them, the LEP limits are most strongly constraining the parameter space. Especially, when $\phi'_\kappa = 90^\circ$ only a small region with $0.25 \lesssim |\lambda| \lesssim 0.35$ and $|\kappa| \lesssim 0.2$ is allowed after including the chargino mass limit. In Fig. 8, we show the allowed region in the $|A_\kappa|$ - $|A_\lambda|$ plane taking $|\lambda| = 0.3$ GeV and $|\kappa| = 0.15$. The allowed range of $|A_\lambda|$ is around ~ 1100 GeV when $\phi'_\kappa = 0^\circ$ and it moves to a higher-value region as ϕ'_κ increases, similar to the scenario considered in the previous section. The LEP limits and the positivity condition of $M_H^2 > 0$ constrain the parameter space $|A_\kappa| \lesssim 250$ GeV, and

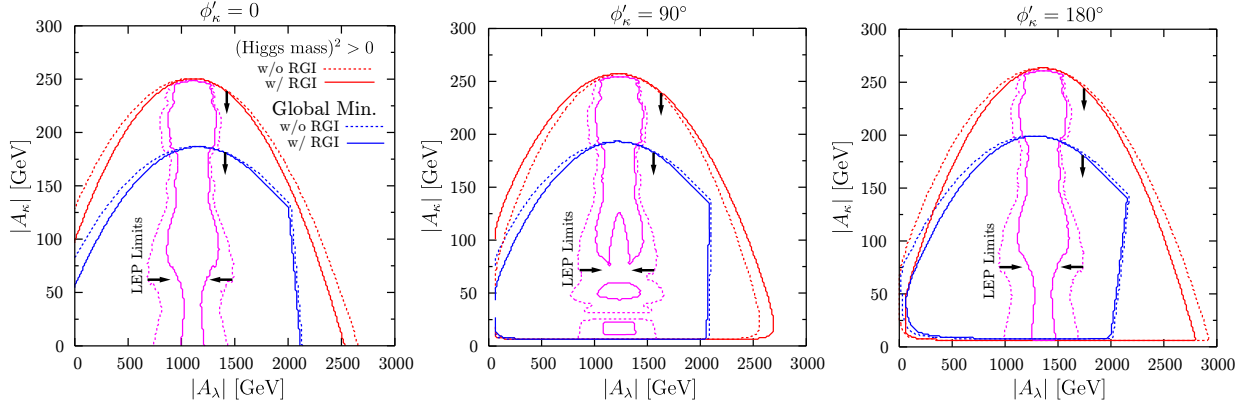


Figure 8: The allowed region in the $|A_\kappa|$ - $|A_\lambda|$ plane for the scenario (4.5) with $|\lambda| = 0.3$ and $|\kappa| = 0.15$ for the three values of $\phi'_\kappa = 0^\circ, 90^\circ$, and 180° . The lines are the same as in Fig. 1.

it is further constrained to $|A_\kappa| \lesssim 200$ GeV by the global minimum condition. Additional restriction arises for small $|A_\kappa|$ when $\phi'_\kappa = 90^\circ, 180^\circ$.

To understand why the LEP limits become stronger with the RG improvement and why the allowed region shows interesting features when $\phi'_\kappa = 90^\circ$ (see the middle frame of Fig. 8), we examine the three light Higgs-boson masses and their couplings to a pair of vector bosons. In Fig. 9, we show the masses (left panel) and couplings (right panel) as functions of $|A_\kappa|$ taking $|A_\lambda| = 1200$ GeV. In the left panels, the dotted lines are for the masses without the RG improvement. The lightest Higgs-boson mass becomes negative when $|A_\kappa| \gtrsim 250$ GeV, signaling the tachyonic state. For $\phi'_\kappa = 0$ (upper panels), two level crossings happen at $|A_\kappa| = 50$ GeV and ~ 70 GeV. Below $|A_\kappa| \lesssim 50$ GeV, H_1 (blue lines) is CP odd and the RG improvement pushes down the mass of H_2 (black lines) to make the LEP limit stronger. When $|A_\kappa|$ is between ~ 50 GeV and ~ 70 GeV, H_2 is CP odd and H_1 is near to the LEP limit with sizable coupling $g_{H_1 V V}^2 \gtrsim 10^{-1}$. When $|A_\kappa| \gtrsim 70$ GeV, H_3 is CP odd and the RG improvement decreases the mass of H_2 by the amount of ~ 10 GeV but M_{H_2} is still above the LEP limit, though very near to it. When $\phi'_\kappa = 90^\circ$ (lower panels), the three states do not carry definite CP parities and $g_{H_2 V V}^2$ is the largest when $|A_\kappa|$ is below 35 GeV and above 75 GeV, explaining the large correction to M_{H_2} (black) there. Between $|A_\kappa| = 35$ GeV and 75 GeV, $g_{H_3 V V}^2$ is the largest and M_{H_3} (red) is affected by the RG improvement most significantly. We note that $g_{H_1 V V}^2$ is enhanced in the region around $|A_\kappa| = 70$ GeV. This explains why the region is ruled out by the LEP limits, while allowed in the CP-conserving case.

In Fig. 10, we show the masses (left panels) and the couplings (right panels) of the light three Higgs bosons as functions of $|A_\lambda|$ taking $|A_\kappa| = 130$ GeV. Around $|A_\lambda| \sim 1200$ GeV, in both cases with $\phi'_\kappa = 0^\circ$ and 90° , $g_{H_2 V V}^2$ (black lines) is the largest and the RG

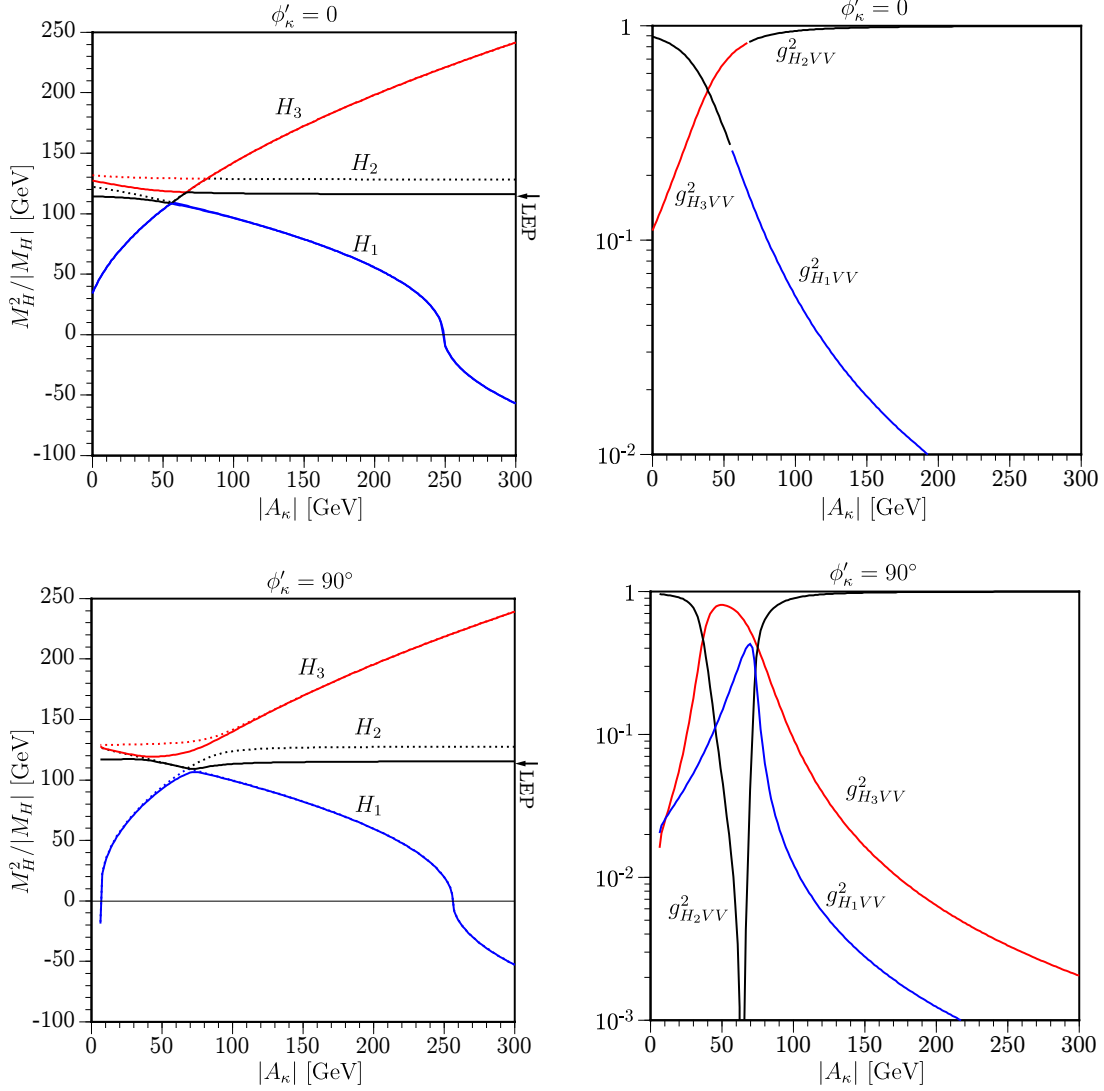


Figure 9: The masses $M_{H_i}^2/|M_{H_i}|$ (left panels) and couplings $g_{H_i V V}^2$ (right panels) for $i = 1, 2, 3$ as functions of $|A_\kappa|$ taking $|A_\lambda| = 1200$ GeV for the scenario in Eq. (4.5). The global minimum condition constrains $|A_\kappa|$ as $0 \leq |A_\kappa| \lesssim 185$ GeV ($\phi'_\kappa = 0^\circ$, upper panels) and $7 \text{ GeV} \lesssim |A_\kappa| \lesssim 192$ GeV ($\phi'_\kappa = 90^\circ$, lower panels).

improvement decreases the mass of H_2 and increases the mixing between H_1 and H_2 states, making the LEP limits stronger. We observe that the LEP limits allows only the region around $|A_\lambda| \sim 1200$ GeV since when moving away from the point, the mass of H_1 decreases while its coupling is rapidly increasing.

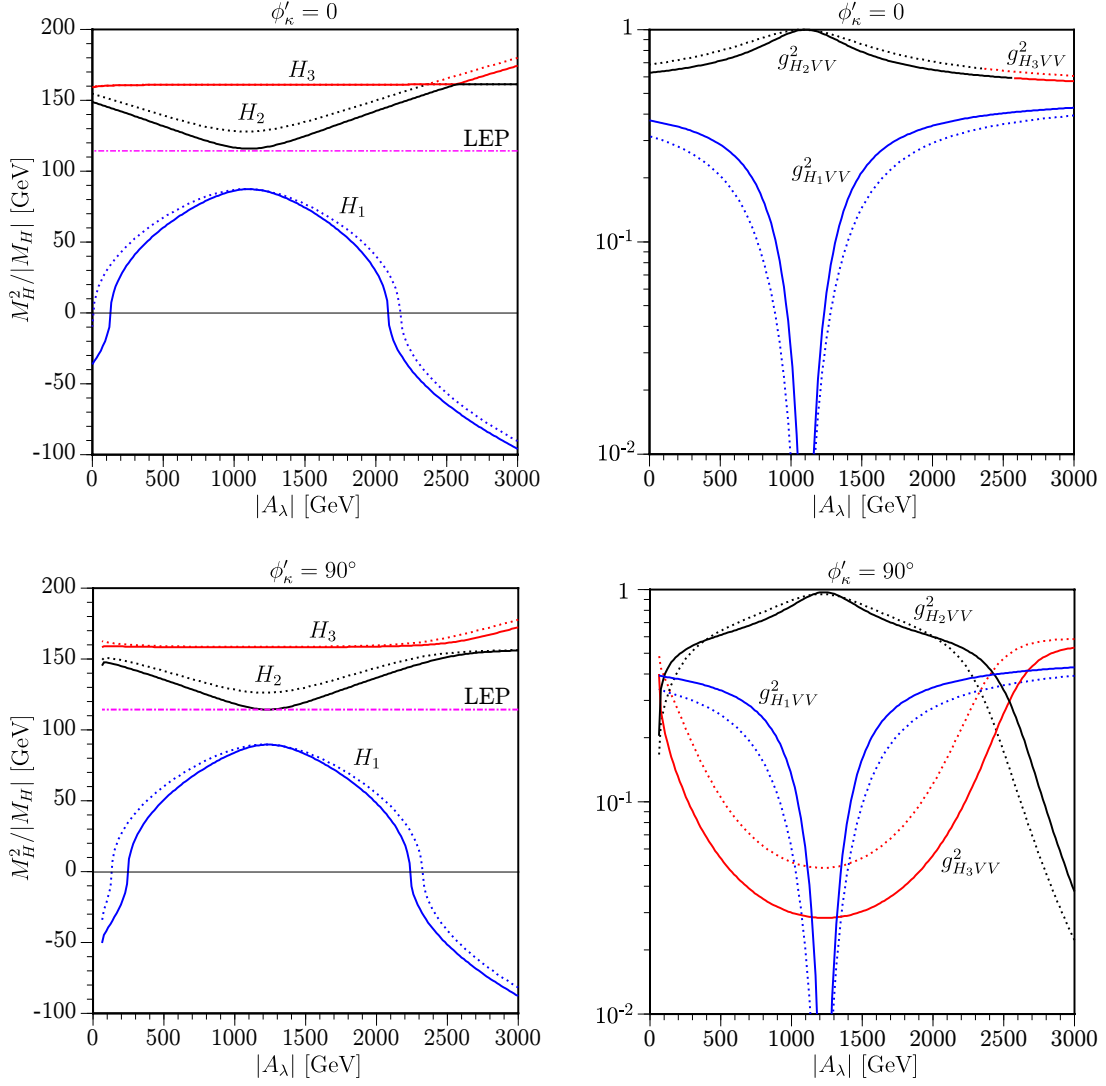


Figure 10: The masses $M_{H_i}^2/|M_{H_i}|$ (left panels) and couplings $g_{H_i V V}^2$ (right panels) for $i = 1, 2, 3$ as functions of $|A_\lambda|$ taking $|A_\kappa| = 130$ GeV for the scenario in Eq. (4.5). The global minimum condition constrains $|A_\lambda|$ as 400 (305) GeV $\lesssim |A_\lambda| \lesssim 1995$ (2018) GeV ($\phi'_\kappa = 0^\circ$, upper panels) and 426 (328) GeV $\lesssim |A_\lambda| \lesssim 2073$ (2092) GeV ($\phi'_\kappa = 90^\circ$, lower panels) with (without) the RG improvement.

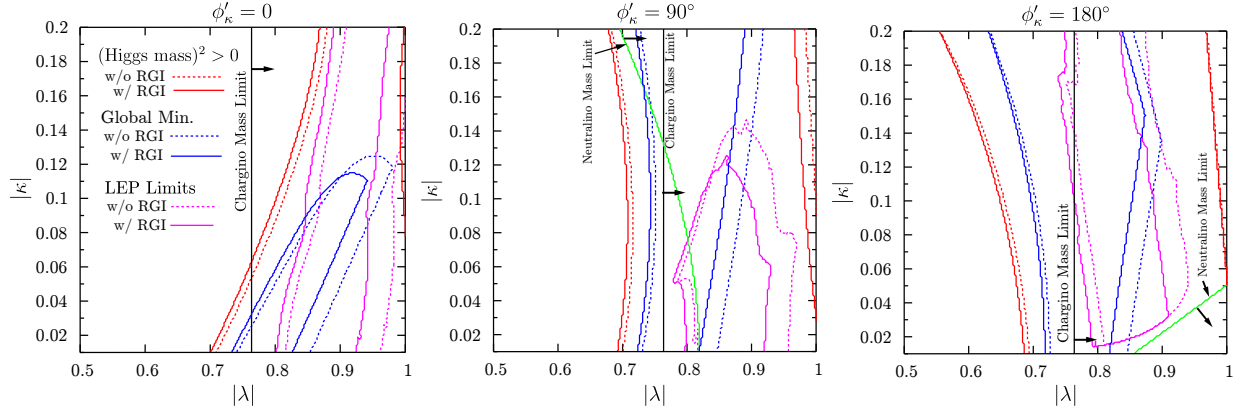


Figure 11: The allowed region in the $|\kappa|$ - $|\lambda|$ plane for the scenario in Eq. (4.7) with $|A_\lambda| = 600$ GeV and $|A_\kappa| = 125$ GeV. The lines are the same as in Fig. 1.

4.3 An electroweak baryogenesis (EWBG)-motivated scenario

The last scenario we are considering has an intermediate value of $\tan \beta$ with small v_S :

$$\begin{aligned}
 \tan \beta &= 5, \quad v_S = 200 \text{ GeV}, \\
 M_{\tilde{Q}} &= M_{\tilde{U}} = M_{\tilde{D}} = |A_t| = |A_b| = 1000 \text{ GeV}, \\
 \phi'_\lambda &= 0, \\
 \text{sign} [\cos(\phi'_\kappa + \phi_{A_\kappa})] &= \text{sign} [\cos(\phi'_\lambda + \phi_{A_\lambda})] = +1,
 \end{aligned} \tag{4.7}$$

while varying

$$|\lambda|, |\kappa|; |A_\lambda|, |A_\kappa|; \phi'_\kappa, \phi_A, \tag{4.8}$$

where $\phi_A \equiv \phi_{A_t} = \phi_{A_b}$ denotes the common CP phase of the third-generation trilinear terms. If it is not mentioned otherwise, we are taking $\phi_A = 0$. We have fixed $M_1 = M_2 = -200$ GeV as in the previous cases. We find that a first-order phase transition could occur in some regions of the parameter space of this scenario [25], which is needed for the EWBG [36].

In Fig. 11, we show the allowed region in the $|\kappa|$ - $|\lambda|$ plane taking $|A_\lambda| = 600$ GeV and $|A_\kappa| = 125$ GeV for the three values of $\phi'_\kappa = 0^\circ$ (left panel), 90° (middle panel), and 180° (right panel). Again, we observe that the allowed region is largely affected by the CP phase and the RG improvement. The RG improvement tends to shift the allowed region to lower values of $|\lambda|$. The $|\kappa|$ is bounded above by ~ 0.12 when $\phi'_\kappa = 90^\circ$. In Fig. 12, the allowed region is shown in the $|A_\kappa|$ - $|A_\lambda|$ plane taking $|\lambda| = 0.83$ ^{||} and $|\kappa| = 0.05$ for

^{||} It was shown in Ref. [26] that a $|\lambda| = 0.7$ at the weak scale is perfectly safe with perturbativity below the grand unified theory (GUT) scale, while we have verified that a $|\lambda| = 0.8$ at the weak scale still gives a value below 4π at the GUT scale. Therefore, the value $|\lambda| = 0.83$ chosen is not expected to have any serious violation of perturbativity up to the GUT scale.

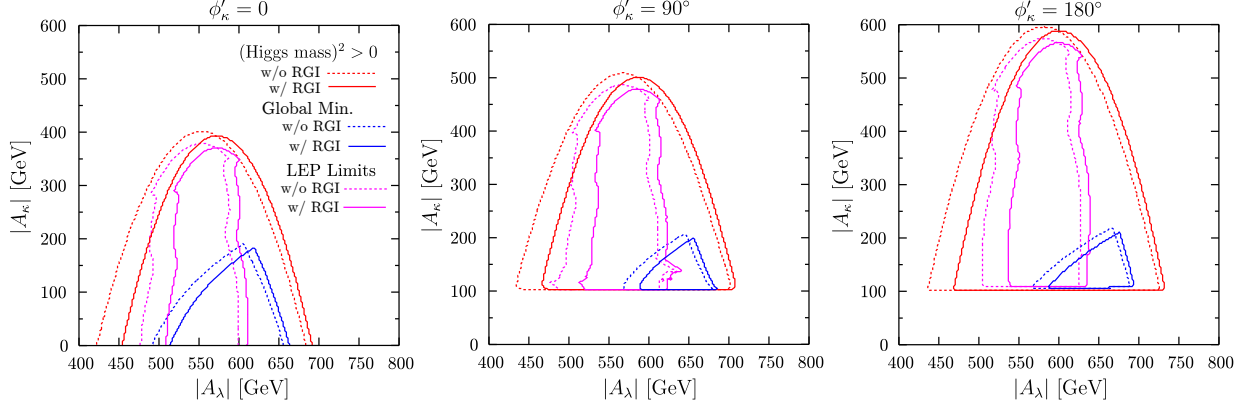


Figure 12: The allowed region in the $|A_\kappa|$ - $|A_\lambda|$ plane for the scenario in Eq. (4.7) with $|\lambda| = 0.83$ and $|\kappa| = 0.05$. The lines are the same as in Fig. 1.

the three values of $\phi'_\kappa = 0^\circ$ (left panel), 90° (middle panel), and 180° (right panel). The RG improvement tends to shift the allowed region to higher values of $|A_\lambda|$ and the global minimum condition is stronger when $\phi'_\kappa = 90^\circ$ and 180° , leaving a small allowed region with $100 \text{ GeV} \lesssim |A_\kappa| \lesssim 200 \text{ GeV}$ around $|A_\lambda| \sim 600 \text{ GeV}$.

In Fig. 13, we show the masses (left panels) and couplings (right panels) as functions of $|A_\lambda|$ taking $|A_\kappa| = 125 \text{ GeV}$. The dotted lines are for the masses and couplings without the RG improvement. We see that the RG improvement shifts the masses and couplings to the region with larger values of $|A_\lambda|$.

In Fig. 14, we show the masses (left panels) and couplings (right panels) as functions of $|A_\kappa|$ (ϕ'_κ) at $\phi'_\kappa = 90^\circ$ ($|A_\kappa| = 140 \text{ GeV}$) in the upper (lower) frames. We have fixed $|A_\lambda| = 625 \text{ GeV}$, because for this value the RG improvement could significantly enlarge the allowed region as seen from the middle and right panels of Fig. 12. Before including the RG improvement, as bounded by the dotted vertical lines, the allowed region is very narrow:

$$\begin{aligned}
 137 \text{ GeV} \lesssim |A_\kappa| \lesssim 144 \text{ GeV} & \quad \text{when} \quad \phi'_\kappa = 90^\circ & \quad (\text{upper}) \\
 88^\circ \lesssim \phi'_\kappa \lesssim 93^\circ & \quad \text{when} \quad |A_\kappa| = 140 \text{ GeV} & \quad (\text{lower}).
 \end{aligned}$$

While, including the RG improvement, the allowed region is enlarged as:

$$\begin{aligned}
 124 \text{ GeV} \lesssim |A_\kappa| \lesssim 152 \text{ GeV} & \quad \text{when} \quad \phi'_\kappa = 90^\circ & \quad (\text{upper}) \\
 82^\circ \lesssim \phi'_\kappa \leq 180^\circ & \quad \text{when} \quad |A_\kappa| = 140 \text{ GeV} & \quad (\text{lower}).
 \end{aligned}$$

This is because the couplings to the weak gauge bosons are on the verge of the LEP-allowed region and the size of the couplings are generically reduced by the RG improvement, as seen from the right panels of Fig. 12.

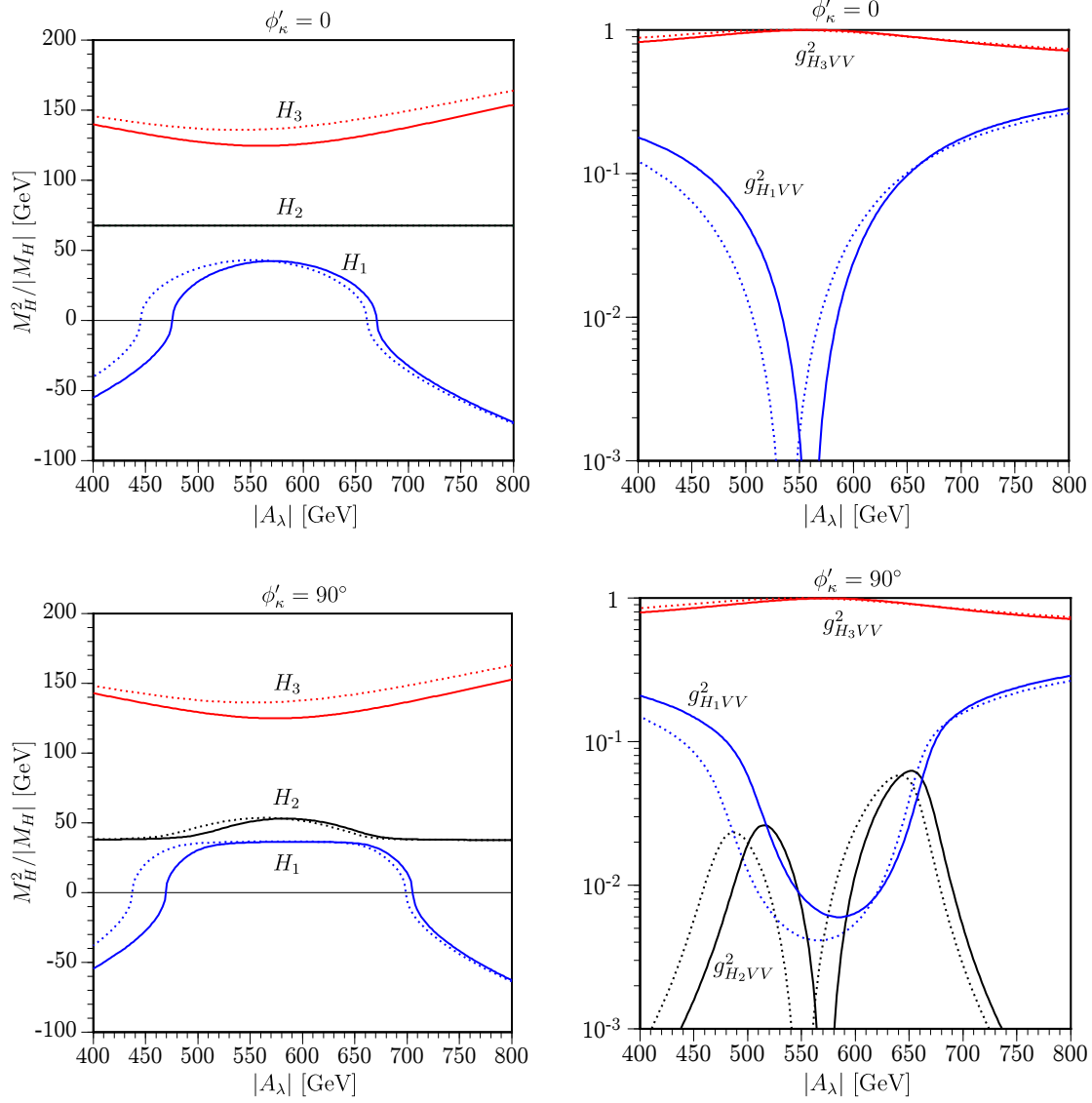


Figure 13: The masses $M_{H_i}^2/|M_{H_i}|$ (left panels) and couplings $g_{H_i V V}^2$ (right panels) as functions of $|A_\lambda|$ taking $|A_\kappa| = 125$ GeV for the scenario in Eq. (4.7) with $|\lambda| = 0.83$, $|\kappa| = 0.05$. The global minimum condition constrains $|A_\lambda|$ as $551 \text{ GeV} \lesssim |A_\lambda| \lesssim 625 \text{ GeV}$ ($\phi'_\kappa = 0^\circ$ without the RGI), $571 \text{ GeV} \lesssim |A_\lambda| \lesssim 634 \text{ GeV}$ ($\phi'_\kappa = 0^\circ$ with the RGI); $576 \text{ GeV} \lesssim |A_\lambda| \lesssim 668 \text{ GeV}$ ($\phi'_\kappa = 90^\circ$ without the RGI), $596 \text{ GeV} \lesssim |A_\lambda| \lesssim 675 \text{ GeV}$ ($\phi'_\kappa = 90^\circ$ with the RGI).

Finally, we study the effect of ϕ_A , the common CP phase of the third-generation trilinear terms. Being different from the previous LEP-compatible scenario in Eq. (4.5), we find that the EWBG-motivated scenario in Eq. (4.7) is sensitive to ϕ_A . In Fig. 15, we show the dependence of the allowed region in the $|\kappa|$ - $|\lambda|$ plane on ϕ_A taking $|A_\lambda| = 600$

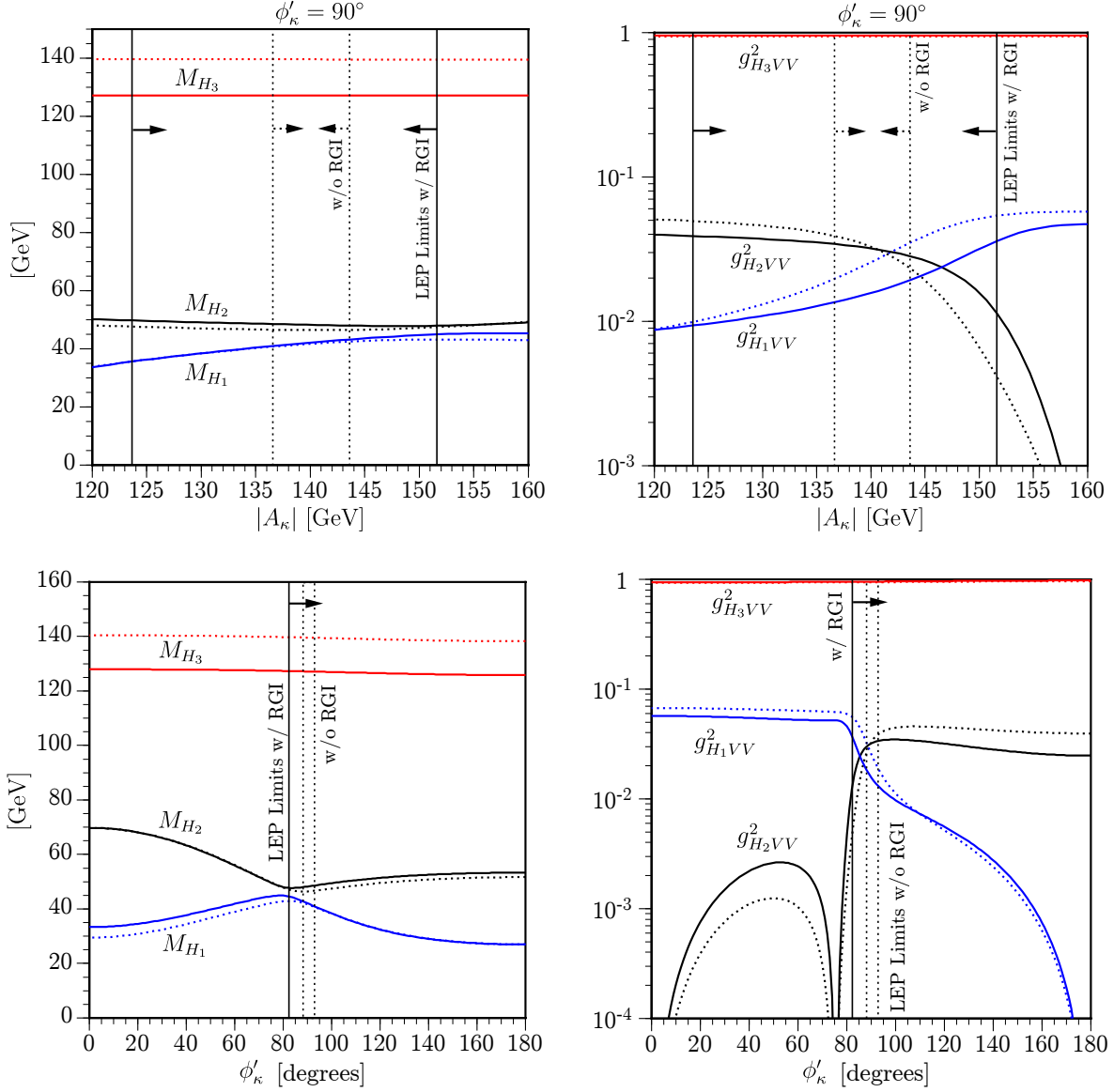


Figure 14: (Upper panels) The masses M_{H_i} (left panels) and couplings $g^2_{H_iVV}$ (right panels) for $i = 1, 2, 3$ as functions of $|A_\kappa|$ taking $|A_\lambda| = 625$ GeV and $\phi'_\kappa = 90^\circ$ for the scenario in Eq. (4.7) with $|\lambda| = 0.83$, $|\kappa| = 0.05$. (Lower panels) The same as in the upper panels but as functions of ϕ'_κ taking $|A_\kappa| = 140$ GeV. The vertical solid and dotted lines bound the allowed region with and without the RGI, respectively.

GeV and $|A_\kappa| = 125$ GeV for the three values of $\phi'_\kappa = 0^\circ$ (upper panel) and 90° and 180° (lower panels). The RG improvement has been included in all cases. The solid lines are for $\phi_A = 90^\circ$ while the dashed lines are for $\phi_A = 0^\circ$ which are the same as the solid lines in Fig. 11 with the RGI. The bounding lines from the condition $M_H^2 > 0$ are not shown here because the condition is always weaker than the LEP limits in this case. We observe

that the allowed regions prefer lower $|\lambda|$ values when $\phi_A = 90^\circ$. For $\phi'_\kappa = 0^\circ$ and 90° there is no region in which the global minimum condition and the LEP limits can be satisfied simultaneously for both values of ϕ_A . In Fig. 16, we show the dependence of the Higgs masses and couplings on ϕ_A at $\phi'_\kappa = 0^\circ$. This figure illustrates the interesting case in which the CP-conserving limits with $\phi_A = 0^\circ$ and 180° are not compatible with the LEP limits. The specific parameter set chosen satisfies the LEP constraints only with nontrivial ϕ_A . This is because a parametric cancellation occurs between the two terms contributing to the coupling $g_{H_1VV} = O_{11}c_\beta + O_{21}s_\beta$ around $\phi_A = 90^\circ$, leading to the suppression of the coupling, as shown in the right panel.

5 Conclusions

We have performed a comprehensive study on the mass spectrum, mixing, and couplings to weak gauge bosons of the Higgs sector within the NMSSM, which is a gauge singlet extension of the MSSM with Z_3 symmetry to address the μ problem. The CP-violating parameters in the superpotential and in the soft SUSY-breaking terms are fully taken into account.

At the tree level, there are three rephasing invariant combinations of the CP phases, two of which are fixed by the CP-odd tadpole conditions up to a twofold ambiguity. In contrast to the MSSM, there still remains one physical CP phase, which induces the tree-level CP-violating mixing among the 5 neutral Higgs states. Apart from the CP phase ($\phi'_\lambda - \phi'_\kappa$), the tree-level Higgs sector is completely determined by the additional 7 real parameters: (i) magnitudes of the two couplings, $|\lambda|$ and $|\kappa|$, (ii) the three VEVs, v_u , v_d , and v_S (or v , $\tan\beta$, and v_S), and (iii) magnitudes of the two A terms, $|A_\lambda|$ and $|A_\kappa|$. With the general notion of the tree-level CP-violating mixing in the neutral Higgs sector, we derive a perturbative way to block-diagonalize a symmetric $(n+m) \times (n+m)$ matrix iteratively and present analytic expressions for the leading-order effects for the CP-violating mixing when the perturbative expansion of the mass matrix works reasonably.

We have computed the masses and mixing matrix of the Higgs bosons at one-loop level using the effective potential method. We have taken into account the CP phases of the stop and sbottom sectors, which enter through the combinations of $\phi'_\lambda + \phi_{A_t}$ and $\phi'_\lambda + \phi_{A_b}$. We also include the logarithmically enhanced two-loop corrections of the order $\mathcal{O}(g_s^2 h^4)$ and $\mathcal{O}(h^6)$ by performing the RG improvement of the one-loop effective potential, which has been implemented only in the CP-conserving limit before. Beyond tree level our results are in agreement with those in the literature, in the CP-conserving limit [32] and in the case of without renormalization-group improvement [29].

In our numerical analyses, we have considered the following three different scenarios:

$$\begin{aligned}
\text{S1 (Typical)} &: & \tan\beta = 3, & \quad v_S = 750 \text{ GeV} \\
\text{S2 (LEP-compatible)} &: & \tan\beta = 10, & \quad v_S = 600 \text{ GeV} \\
\text{S3 (EWBG-motivated)} &: & \tan\beta = 5, & \quad v_S = 200 \text{ GeV}
\end{aligned}$$

We have chosen the phase convention with $\phi'_\lambda = 0$ and varied $|\lambda|, |\kappa|$; $|A_\lambda|, |A_\kappa|$; $\phi'_\kappa, \phi_A = \Phi_{A_t, A_b}$. For the SUSY-breaking parameters we have fixed $M_{\tilde{Q}} = M_{\tilde{U}} = M_{\tilde{D}} = |A_t| = |A_b| = 1 \text{ TeV}$ and, for other parameters, we refer to Eqs. (4.2), (4.5), and (4.7). In each scenario, the following three main conditions are imposed to derive constraints on the parameter space: (i) the LEP limits, (ii) the global minimum condition, and (iii) the positivity of the Higgs-boson masses squared. The third condition is always weaker than the other two. The global minimum condition does not allow too large values for the trilinear parameters $|A_\lambda|$ and $|A_\kappa|$ because the energy of the presumed EW vacuum is proportional to them. The LEP limits constrain the allowed parameter space around $|A_\lambda| \sim |\lambda|v_S t_\beta / \sqrt{2}$, which is also the typical size of the heavier Higgs bosons. The relative strength of the global minimum condition and the LEP limits depends on the scenarios.

The renormalization-group improvement included in this study substantially strengthens the LEP limits, thus making it more restrictive. In the typical scenario S1, the allowed region of the parameter space strongly depends on the CP phase ϕ'_κ and the RG improvement. We found that the typical points with small $|\lambda|$ and $|\kappa|$, which are allowed before the inclusion of the RG improvement, are completely ruled out by the LEP limits after including the RG improvement. In the LEP-compatible scenario S2, the allowed region of the parameter space also strongly depends on the CP phase ϕ'_κ and the RG improvement but the dependence on ϕ_A is weak. We observe that the RG-improved correction reduces the mass of the SM-like Higgs boson by an amount of a few GeV to about 10 GeV, increases the mixing between the lighter states, and shrinks the allowed parameter space significantly. When ϕ'_κ takes on nontrivial values, the lighter states do not carry definite CP parities and the shape of the allowed parameter region becomes more complicated compared to the CP-conserving case. Last, in the EWBG-motivated scenario S3, we find that the global minimum condition restricts the parameter space more tightly than the LEP limits and some parameter region, which is not allowed in the CP-conserving case, could be allowed by assuming nontrivial values of ϕ'_κ and ϕ_A , enlarging the allowed parameter space.

We offer a few more comments before closing such as the following:

1. This is the first time that the next-to-minimal supersymmetric standard model is studied allowing CP phases in the μ and soft SUSY-breaking parameters, and including full one-loop corrections with renormalization-group improvement. Substantial corrections to the Higgs-boson spectrum, mixing, and couplings to weak gauge bosons are realized. Furthermore, nontrivial variations in the mass spectrum, mixing, and

couplings appear due to nonzero CP phases. Therefore, we anticipate a whole new set of phenomenology associated within this CP-violating NMSSM framework.

2. It is well known that the experimental measured EDMs place nontrivial constraint on the CP phases. With one more physical CP phase added in this NMSSM framework the predictions for EDMs are important to constrain the combinations of phases [37]. Such CP phases are also important to provide enough CP violation required in the electroweak baryogenesis.
3. A successful supersymmetry model should be able to explain the anomalous magnetic moment of the muon, which is widely accepted as a 3σ effect [38]. The CP-violating NMSSM considered in this work should also be constrained so as to satisfy the muon anomaly. It is a nontrivial extension in this regard because of the presence of many new Higgs bosons, which can be very light and with CP violating couplings.
4. There are a number of low-energy constraints on the lightest CP-odd Higgs boson in the CP-conserving NMSSM [39]. The exercises can be repeated in the presence of the new CP phases.
5. There are a number of important cubic terms in the Higgs potential, which also have nontrivial dependence on the Higgs spectrum and CP phases. Specifically, for successful baryogenesis, the soft cubic term involving the singlet field $\lambda A_\lambda S H_d H_u + \text{h.c.}$, which is absent in the MSSM, is vital to enable a first-order phase transition when the stops are heavy. Apparently, from the EWBG-motivated scenario studied in this work, a first-order phase transition is possible in this framework. We will delay this issue to a detailed study in the future [37]
6. A whole new set of phenomenology has to be explored in the Higgs sector with 5 neutral Higgs bosons with no definite CP parities, and a pair of charged Higgs bosons. As we can see in this work, the couplings to weak gauge bosons vary nontrivially with the CP phases. The same can be said for the mass spectrum. It is more complicated than the CP-violating MSSM or CP-conserving NMSSM. At this point, we cannot forecast how the decay branching ratios and production will be modified. We delay this to a further study.
7. With CP violation there is no explicit CP property for the Higgs bosons. In most of the cases, there are three relatively light neutral Higgs bosons and two relatively heavy ones. The collider phenomenology is particularly concerned with the three lighter ones, in which one of them is the SM-like Higgs boson with a relatively large coupling to the gauge bosons than the other two Higgs bosons (but still the strength is a fraction of the SM value.) At the Tevatron, the most useful Higgs production channel is via the associated production with a W or a Z boson. The production

rate of the SM-like Higgs boson is smaller than the corresponding SM Higgs boson, but it may be possible to produce more than one Higgs boson. At the LHC, on the other hand, production is dominated by the gluon fusion. The crucial strategies for Higgs-boson search depend on the decay pattern of the Higgs bosons.

8. There are a number of possible channels that the SM-like Higgs boson can decay into, including the dominant $b\bar{b}$, $\tau^+\tau^-$, the rare ones $\mu^+\mu^-$, $\gamma\gamma$, $Z\gamma$, and the possible new ones h_1h_1 , h_1h_2 , and h_2h_2 depending on the mass spectrum. In the CP-conserving NMSSM, the SM-like Higgs boson can decay into 2 CP-even lighter Higgs bosons or 2 CP-odd Higgs bosons, but not a mixture. Now with CP violation, the SM-like Higgs boson can decay into h_1h_2 , which is not possible in the CP-conserving case. It is a clean signal of CP violation. Further decays of h_1 and h_2 will give a total of four fermions in the final state, e.g., $4b$, $2b2\tau$, 4τ , 4μ , $2\mu2\tau$, $2b2\mu$, etc. Feasibility and coverage of parameter space certainly deserve further studies.

We conclude by summarizing that we have started a new avenue in the CP-violating NMSSM, which involves a whole new set of phenomenology in low-energy precision measurements, in the LHC Higgs-boson searches, baryogenesis, etc., to be explored in the future.

Acknowledgements

We thank Koichi Funakubo for helpful discussions. The work was supported in parts by the NSC of Taiwan (96-2628-M-007-002-MY3), the NCTS, and by the WCU program through the KOSEF funded by the MEST (R31-2008-000-10057-0).

A Appendix

In this Appendix, we consider a block diagonalization of a symmetric $(n+m) \times (n+m)$ matrix

$$S = \begin{pmatrix} A & C \\ C^T & B \end{pmatrix}, \quad (\text{A.1})$$

where the submatrices can be expanded as

$$A \equiv A_0 + \sum_{n=1} \epsilon^n A_n \quad ; \quad B \equiv \sum_{n=1} \epsilon^n B_n \quad ; \quad C \equiv \sum_{n=1} \epsilon^n C_n. \quad (\text{A.2})$$

Note that, for successful diagonalization, we require the off-diagonal $n \times m$ submatrix C and the lower $m \times m$ submatrix B to be suppressed by, at least, one power of ϵ compared

with the upper diagonal $n \times n$ submatrix A . The block diagonalization can be implemented by introducing the mixing matrix

$$V = \begin{pmatrix} \mathbf{1}_{n \times n} + y & x \\ -x^T & \mathbf{1}_{m \times m} + z \end{pmatrix}, \quad (\text{A.3})$$

where the submatrices in the diagonal parts are symmetric, $y^T = y$ and $z^T = z$, and all three submatrices can also be expanded as **

$$x \equiv \sum_{n=1} \epsilon^n x_n ; \quad y \equiv \sum_{n=2} \epsilon^n y_n ; \quad z \equiv \sum_{n=2} \epsilon^n z_n. \quad (\text{A.4})$$

Using the orthogonality of the matrix V , $VV^T = V^TV = \mathbf{1}_{(n+m) \times (n+m)}$, we impose the relations

$$2y + y^2 + xx^T = \mathbf{0}_{n \times n} ; \quad 2z + z^2 + x^T x = \mathbf{0}_{m \times m} ; \quad yx = xz, \quad (\text{A.5})$$

which can be used to determine the diagonal matrices y and z in terms of x iteratively, order by order in ϵ , as follows:

$$\begin{aligned} y_2 &= -\frac{1}{2} x_1 x_1^T \\ y_3 &= -\frac{1}{2} (x_1 x_2^T + x_2 x_1^T) \\ y_4 &= -\frac{1}{2} (x_1 x_3^T + x_3 x_1^T + x_2 x_2^T) - \frac{1}{8} (x_1 x_1^T)^2 \\ &\dots \\ y_i &= y_i(x_1, x_2, \dots, x_{i-1}) \end{aligned} \quad (\text{A.6})$$

and

$$z_i = y_i(x_j \rightarrow x_j^T \text{ for } j < i) \quad (\text{A.7})$$

Therefore, to determine the diagonal entries of the mixing matrix V up to order ϵ^i , all we need to know is $(x_1, x_2, \dots, x_{i-1})$ which can be obtained by requiring the off-diagonal part of VSV^T to vanish, order by order in ϵ up to ϵ^{i-1} , and in terms of the submatrices $A_{0,1,\dots,(i-1)}$, $B_{1,\dots,(i-1)}$, and $C_{1,2,\dots,(i-1)}$.

More specifically we define the block-diagonal matrix

$$\tilde{S} \equiv VSV^T = \begin{pmatrix} \tilde{S}_{11} & \tilde{S}_{12} \\ \tilde{S}_{12}^T & \tilde{S}_{22} \end{pmatrix}, \quad (\text{A.8})$$

**Note that y and z starts from the second order of ϵ , required by the ϵ expansion of the off-diagonal part x of V and the orthogonality of the mixing matrix V , as shown below.

with

$$\begin{aligned}\tilde{S}_{11} &= A + (Ay + yA + Cx^T + xC^T) + xBx^T + (yAy + yCx^T + xC^T y) \\ \tilde{S}_{22} &= B + (x^T Ax - C^T x - x^T C) + (Bz + zB) + (-zC^T x - x^T Cz) + zBz\end{aligned}\quad (\text{A.9})$$

in order of increasing power in ϵ of the leading terms. The vanishing off-diagonal part is

$$\tilde{S}_{12} = (-Ax + C) + xB + (-yAx - xC^T x + yC + Cz) + xBz + yCz, \quad (\text{A.10})$$

where the first, the second, the third, the fourth, and the fifth term starts from ϵ^1 , ϵ^2 , ϵ^3 , ϵ^4 , and ϵ^5 , respectively. To solve $\tilde{S}_{12} = \mathbf{0}_{n \times m}$, we have made the following rearrangement:

$$\tilde{S}_{12} = \sum_{i=1} \epsilon^i \left(\tilde{S}_{12} \right)_i \equiv \sum_{i=1} \epsilon^i (-A_0 x_i + C_i + D_i), \quad (\text{A.11})$$

where D_i 's are functions of A , B , C , and $(x_1, x_2, \dots, x_{i-1})$:

$$D_i = D_i(x_j; A_j, B_j, C_j) \text{ with } j < i. \quad (\text{A.12})$$

Therefore, $(\tilde{S}_{12})_i = \mathbf{0}_{n \times m}$ can be solved iteratively to give x_i :

$$x_i = A_0^{-1} (C_i + D_i) \quad (\text{A.13})$$

Here, for example, we give a few first D_i 's:

$$\begin{aligned}D_1 &= 0 \\ D_2 &= -A_1 x_1 + x_1 B_1 \\ D_3 &= -A_1 x_2 - A_2 x_1 + x_2 B_1 + x_1 B_2 - \frac{1}{2} C_1 x_1^T x_1 - \frac{1}{2} x_1 x_1^T C_1 - x_1 C_1^T x_1 + \frac{1}{2} x_1 x_1^T A_0 x_1.\end{aligned}\quad (\text{A.14})$$

This completes the block diagonalization of the symmetric matrix S . To summarize, assuming all the x_j 's are known up to $j = i - 1$, x_i can be easily obtained by solving $(\tilde{S}_{12})_i = \mathbf{0}_{n \times m}$ and then (x_1, x_2, \dots, x_i) fixes y_{i+1} and z_{i+1} for the mixing matrix and the block-diagonalized matrices up to the ϵ^{i+1} order.

As a simple application of our method, we consider the situation ^{††}

$$A = A_0, \quad B = \epsilon^2 B_2, \quad C = \epsilon C_1. \quad (\text{A.15})$$

In the first order of ϵ ,

$$x_1 = A_0^{-1} C_1, \quad (\text{A.16})$$

which leads to

$$y_2 = -\frac{1}{2} x_1 x_1^T, \quad z_2 = -\frac{1}{2} x_1^T x_1, \quad (\text{A.17})$$

for the mixing matrix and the block-diagonalized matrices are given by

$$\tilde{S}_{11} = A_0 + \frac{1}{2} \epsilon^2 (C_1 x_1^T + x_1 C_1^T); \quad \tilde{S}_{22} = \epsilon^2 (B_2 - C_1^T x_1). \quad (\text{A.18})$$

Note that, in this simple case, x_2 and, accordingly, y_3 and z_3 vanish.

^{††}See, also, the Appendix in Ref. [26].

References

- [1] M. Dine, W. Fischler and M. Srednicki, Phys. Lett. B **104** (1981) 199; H. P. Nilles, M. Srednicki and D. Wyler, Phys. Lett. B **120** (1983) 346; J. M. Frere, D. R. T. Jones and S. Raby, Nucl. Phys. B **222** (1983) 11; A. I. Veselov, M. I. Vysotsky and K. A. Ter-Martirosian, Sov. Phys. JETP **63** (1986) 489 [Zh. Eksp. Teor. Fiz. **90** (1986) 838]; J. P. Derendinger and C. A. Savoy, Nucl. Phys. B **237** (1984) 307.
- [2] J. R. Ellis, J. F. Gunion, H. E. Haber, L. Roszkowski and F. Zwirner, Phys. Rev. D **39** (1989) 844; U. Ellwanger, Phys. Lett. B **303** (1993) 271 [arXiv:hep-ph/9302224]; U. Ellwanger, M. Rausch de Traubenberg and C. A. Savoy, Phys. Lett. B **315** (1993) 331 [arXiv:hep-ph/9307322]; P. N. Pandita, Phys. Lett. B **318** (1993) 338; P. N. Pandita, Z. Phys. C **59** (1993) 575; T. Elliott, S. F. King and P. L. White, Phys. Rev. D **49** (1994) 2435 [arXiv:hep-ph/9308309]; G. K. Yeghiyan, arXiv:hep-ph/9904488; S. F. King and P. L. White, Phys. Rev. D **52** (1995) 4183 [arXiv:hep-ph/9505326]; U. Ellwanger, M. Rausch de Traubenberg and C. A. Savoy, Nucl. Phys. B **492** (1997) 21 [arXiv:hep-ph/9611251]; F. Franke and H. Fraas, Int. J. Mod. Phys. A **12** (1997) 479 [arXiv:hep-ph/9512366]; B. Ananthanarayan and P. N. Pandita, Int. J. Mod. Phys. A **12** (1997) 2321 [arXiv:hep-ph/9601372]; U. Ellwanger and C. Hugonie, Eur. Phys. J. C **25** (2002) 297 [arXiv:hep-ph/9909260]; U. Ellwanger, J. F. Gunion, C. Hugonie and S. Moretti, arXiv:hep-ph/0305109; U. Ellwanger and C. Hugonie, Phys. Lett. B **623** (2005) 93 [arXiv:hep-ph/0504269].
- [3] M. Matsuda and M. Tanimoto, Phys. Rev. D **52** (1995) 3100 [arXiv:hep-ph/9504260]; N. Haba, Prog. Theor. Phys. **97** (1997) 301 [arXiv:hep-ph/9608357]; S. W. Ham, J. Kim, S. K. Oh and D. Son, Phys. Rev. D **64** (2001) 035007 [arXiv:hep-ph/0104144]; S. W. Ham, S. K. Oh and D. Son, Phys. Rev. D **65** (2002) 075004 [arXiv:hep-ph/0110052]; M. Boz, Mod. Phys. Lett. A **21** (2006) 243 [arXiv:hep-ph/0511072]; S. W. Ham, S. H. Kim, S. K. OH and D. Son, Phys. Rev. D **76** (2007) 115013 [arXiv:0708.2755 [hep-ph]].
- [4] G. Degrandi and P. Slavich, Nucl. Phys. B **825**, 119 (2010) [arXiv:0907.4682 [hep-ph]].
- [5] For recent reviews on the NMSSM, see, U. Ellwanger, C. Hugonie and A. M. Teixeira, arXiv:0910.1785 [hep-ph]; S. Chang, R. Dermisek, J. F. Gunion and N. Weiner, Ann. Rev. Nucl. Part. Sci. **58**, 75 (2008) [arXiv:0801.4554 [hep-ph]].
- [6] J. E. Kim and H. P. Nilles, Phys. Lett. B **138**, 150 (1984); Y. Nir, Phys. Lett. B **354**, 107 (1995); M. Cvetič and P. Langacker, Phys. Rev. D **54**, 3570 (1996).
- [7] R. Dermisek and J. F. Gunion, Phys. Rev. Lett. **95**, 041801 (2005); Phys. Rev. D **73**, 111701 (2006); Phys. Rev. D **76**, 095006 (2007); S. Chang, P. J. Fox and N. Weiner, JHEP **0608**, 068 (2006) [arXiv:hep-ph/0511250].

- [8] R. Barate *et al.* [LEP Working Group for Higgs boson searches], Phys. Lett. B **565**, 61 (2003).
- [9] B. A. Dobrescu, G. Landsberg and K. T. Matchev, Phys. Rev. D **63**, 075003 (2001); U. Ellwanger, J. F. Gunion and C. Hugonie, JHEP **0507**, 041 (2005); V. Barger, P. Langacker, H. S. Lee and G. Shaughnessy, Phys. Rev. D **73**, 115010 (2006); S. Chang, P. J. Fox and N. Weiner, Phys. Rev. Lett. **98**, 111802 (2007); V. Barger, P. Langacker and G. Shaughnessy, Phys. Rev. D **75**, 055013 (2007); T. Stelzer, S. Wiesenfeldt and S. Willenbrock, Phys. Rev. D **75**, 077701 (2007) [arXiv:hep-ph/0611242]; K. Cheung, J. Song and Q. S. Yan, Phys. Rev. Lett. **99**, 031801 (2007) [arXiv:hep-ph/0703149]; M. Carena, T. Han, G. Y. Huang and C. E. M. Wagner, JHEP **0804**, 092 (2008) [arXiv:0712.2466 [hep-ph]]; J. Cao, H. E. Logan and J. M. Yang, Phys. Rev. D **79**, 091701 (2009) [arXiv:0901.1437 [hep-ph]]; A. Belyaev, J. Pivarski, A. Safonov, S. Senkin and A. Tatarinov, Phys. Rev. D **81**, 075021 (2010) [arXiv:1002.1956 [hep-ph]].
- [10] B. C. Regan, E. D. Commins, C. J. Schmidt and D. DeMille, Phys. Rev. Lett. **88** (2002) 071805.
- [11] C. A. Baker *et al.*, Phys. Rev. Lett. **97** (2006) 131801.
- [12] M. V. Romalis, W. C. Griffith and E. N. Fortson, Phys. Rev. Lett. **86** (2001) 2505.
- [13] W. C. Griffith, M. D. Swallows, T. H. Loftus, M. V. Romalis, B. R. Heckel and E. N. Fortson, Phys. Rev. Lett. **102** (2009) 101601.
- [14] T. Ibrahim and P. Nath, Phys. Rev. D **58** (1998) 111301 [Erratum-ibid. D **60** (1999) 099902] [arXiv:hep-ph/9807501].
- [15] J. R. Ellis, J. S. Lee and A. Pilaftsis, JHEP **0810** (2008) 049 [arXiv:0808.1819 [hep-ph]].
- [16] A. Pilaftsis, Phys. Rev. D **58** (1998) 096010; Phys. Lett. B **435** (1998) 88.
- [17] A. Pilaftsis and C.E.M. Wagner, Nucl. Phys. B **553** (1999) 3.
- [18] D.A. Demir, Phys. Rev. D **60** (1999) 055006.
- [19] S.Y. Choi, M. Drees and J.S. Lee, Phys. Lett. B **481** (2000) 57; M. Carena, J. Ellis, A. Pilaftsis and C.E.M. Wagner, Nucl. Phys. **B586** (2000) 92; M. Carena, J. Ellis, A. Pilaftsis and C.E.M. Wagner, Nucl. Phys. **B625** (2002) 345.
- [20] J. S. Lee, AIP Conf. Proc. **1078** (2009) 36 [arXiv:0808.2014 [hep-ph]].
- [21] E. Accomando *et al.*, arXiv:hep-ph/0608079.

- [22] S. Y. Choi and J. S. Lee, Phys. Rev. D **61** (1999) 015003 [arXiv:hep-ph/9907496]; S. Y. Choi, K. Hagiwara and J. S. Lee, Phys. Rev. D **64** (2001) 032004 [arXiv:hep-ph/0103294]; S. Y. Choi, M. Drees, J. S. Lee and J. Song, Eur. Phys. J. C **25** (2002) 307 [arXiv:hep-ph/0204200].
- [23] J. S. Lee, A. Pilaftsis, M. Carena, S. Y. Choi, M. Drees, J. R. Ellis and C. E. M. Wagner, Comput. Phys. Commun. **156** (2004) 283 [arXiv:hep-ph/0307377]; J. S. Lee, M. Carena, J. Ellis, A. Pilaftsis and C. E. M. Wagner, Comput. Phys. Commun. **180** (2009) 312 [arXiv:0712.2360 [hep-ph]].
- [24] S. Schael *et al.* [ALEPH Collaboration and DELPHI Collaboration and L3 Collaboration and], Eur. Phys. J. C **47** (2006) 547 [arXiv:hep-ex/0602042].
- [25] K. Funakubo, S. Tao and F. Toyoda, Prog. Theor. Phys. **114**, 369 (2005) [arXiv:hep-ph/0501052].
- [26] D. J. Miller, R. Nevzorov and P. M. Zerwas, Nucl. Phys. B **681** (2004) 3 [arXiv:hep-ph/0304049].
- [27] S. R. Coleman and E. J. Weinberg, Phys. Rev. D **7** (1973) 1888.
- [28] R. Jackiw, Phys. Rev. D **9** (1974) 1686.
- [29] K. Funakubo and S. Tao, Prog. Theor. Phys. **113** (2005) 821 [arXiv:hep-ph/0409294].
- [30] K. Funakubo, S. Tao and F. Toyoda, Prog. Theor. Phys. **109** (2003) 415 [arXiv:hep-ph/0211238].
- [31] H. E. Haber, R. Hempfling and A. H. Hoang, Z. Phys. C **75** (1997) 539 [arXiv:hep-ph/9609331].
- [32] U. Ellwanger, J. F. Gunion and C. Hugonie, JHEP **0502** (2005) 066 [arXiv:hep-ph/0406215]; U. Ellwanger and C. Hugonie, Comput. Phys. Commun. **175** (2006) 290 [arXiv:hep-ph/0508022].
- [33] J. A. Casas, J. R. Espinosa, M. Quiros and A. Riotto, Nucl. Phys. B **436** (1995) 3 [Erratum-ibid. B **439** (1995) 466] [arXiv:hep-ph/9407389].
- [34] W. H. Press, S. A. Teukolsky, W. T. Vetterling and B. P. Flannery, *Numerical Recipes*, (Cambridge University Press, Cambridge, England, 1986).
- [35] G. Abbiendi *et al.* [OPAL Collaboration], Eur. Phys. J. C **35** (2004) 1 [arXiv:hep-ex/0401026].

- [36] For reviews, see A. G. Cohen, D. B. Kaplan and A. E. Nelson, *Ann. Rev. Nucl. Part. Sci.* **43** (1993) 27 [arXiv:hep-ph/9302210]; M. Quiros, *Helv. Phys. Acta* **67** (1994) 451; V. A. Rubakov and M. E. Shaposhnikov, *Usp. Fiz. Nauk* **166** (1996) 493 [*Phys. Usp.* **39** (1996) 461] [arXiv:hep-ph/9603208]; K. Funakubo, *Prog. Theor. Phys.* **96** (1996) 475 [arXiv:hep-ph/9608358]; M. Trodden, *Rev. Mod. Phys.* **71** (1999) 1463 [arXiv:hep-ph/9803479]; W. Bernreuther, *Lect. Notes Phys.* **591** (2002) 237 [arXiv:hep-ph/0205279].
- [37] K. Cheung, T.J. Hou, J.S. Lee, and E. Senaha, in preparation.
- [38] T. Teubner, K. Hagiwara, R. Liao, A. D. Martin and D. Nomura, arXiv:1001.5401 [hep-ph].
- [39] G. Hiller, *Phys. Rev. D* **70**, 034018 (2004) [arXiv:hep-ph/0404220]. R. Dermisek, J. F. Gunion and B. McElrath, *Phys. Rev. D* **76**, 051105 (2007) [arXiv:hep-ph/0612031].

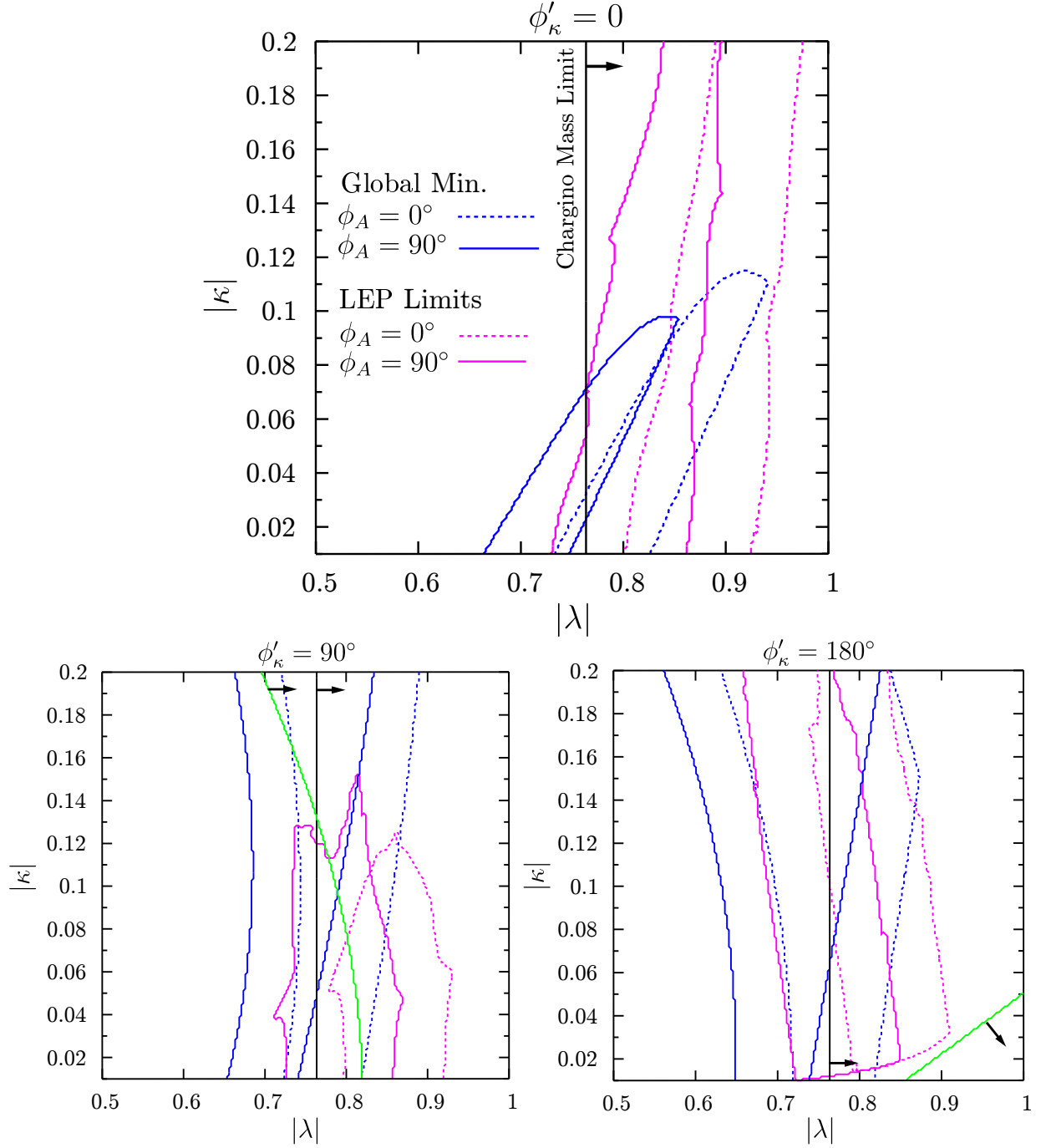


Figure 15: The allowed region in the $|\kappa|$ - $|\lambda|$ plane for the two values of $\phi_A = 0^\circ$ (dashed lines) and 90° (solid lines) taking the scenario in Eq. (4.7) with $|A_\lambda| = 600$ GeV, $|A_\kappa| = 125$ GeV and the three values of $\phi'_\kappa = 0^\circ$ (upper panel) and 90° and 180° (lower panels). The RG improvement has been included in all cases. The dashed lines for $\phi_A = 0^\circ$ are the same as the solid lines in Fig. 11.

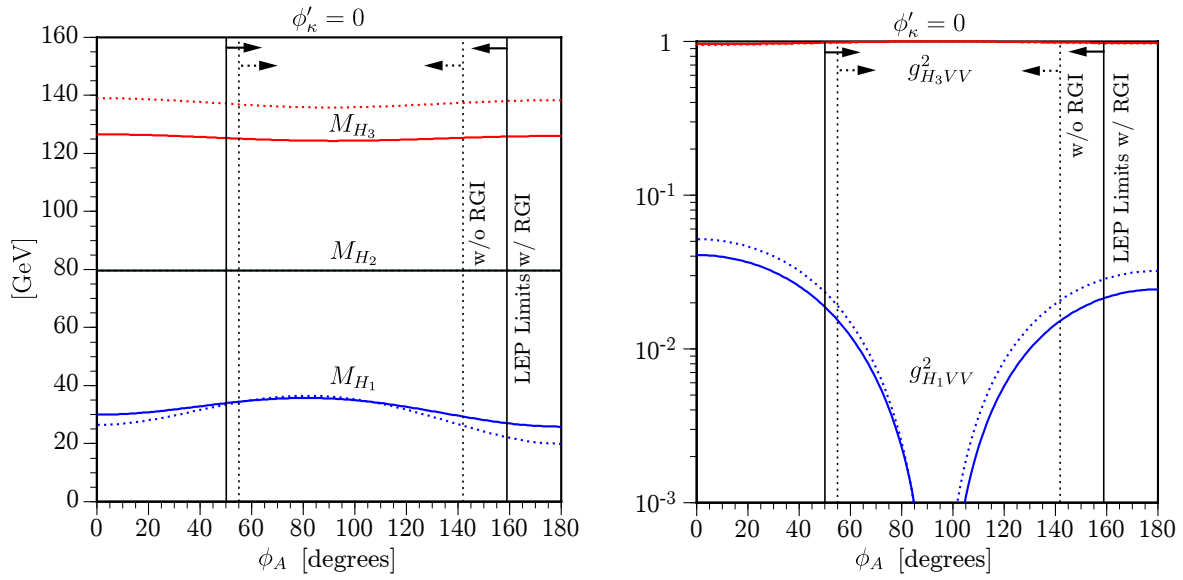


Figure 16: The masses M_{H_i} (left panel) and couplings $g^2_{H_iVV}$ (right panel) for $i = 1, 2, 3$ as functions of ϕ_A taking $|A_\kappa| = 125$ GeV and $|A_\lambda| = 600$ GeV for the scenario in Eq. (4.7) with $|\lambda| = 0.815$, $|\kappa| = 0.07$, and $\phi'_\kappa = 0^\circ$. The vertical solid and dotted lines bound the allowed region with and without the RGI, respectively.